Development and validation of CFD-DEM coupling interface for Heat & Mass Transfer using partitioned coupling approach

Prasad ADHAV[a,*], Xavier BESSERON[a], Alvaro A. ESTUPINAN[a], Bernhard PETERS[a]

[a]*University of Luxembourg, Department of Engineering,*
Maison du Nombre, 6 Avenue de la Fonte, Esch-sur-Alzette, L-4364, Luxembourg

_____

[*]Corresponding author

Email addresses: `prasad.adhav@uni.lu` (Prasad ADHAV),
`xavier.besseron@uni.lu` (Xavier BESSERON), `alvaro@estupinan.net` (Alvaro A.
ESTUPINAN), `bernhard.peters@uni.lu` (Bernhard PETERS)

Abstract

This work demonstrates the rapid development of a simulation environment to achieve Heat and Mass Transfer (HMT) between Discrete Element Method (DEM) and Computational Fluid Dynamics (CFD). This coupling holds potential for simulating various processes like drying, pyrolysis, combustion, melting, and solid-fluid reactions, finding applications in biomass furnaces, boilers, heat exchangers, and flow through packed beds among others. To accurately model these applications, diverse CFD features and solvers must integrate with DEM to capture intricate physics.

The proposed method employs the preCICE coupling library on volumetric meshes, uniting CFD-DEM through an Eulerian-Lagrangian approach for HMT. The prototype uses eXtended Discrete Element Method (XDEM) for DEM calculations and OpenFOAM for CFD. XDEM receives key CFD data fields through preCICE, setting particle boundary conditions based on fluid domain properties and flow conditions. Heat and mass source terms computed by XDEM fed into the CFD solver, representing the particle contributions.

This coupling framework, comprising preCICE, XDEM, and its adapter, accommodates a wide array of applications involving convective heat transfer between particles and fluids. Validation includes comparisons with experiments and a specialized solver, affirming the accuracy of predicted numerical results across heat transfer, drying, and pyrolysis cases. Additionally, the study delves into the computational costs associated with different coupling approaches, offering valuable performance insights.

Keywords: Multi-physics, Coupled Simulations, CFD-DEM, Heat & Mass Transfer, Partitioned Coupling

1. Introduction

The field of engineering faces problems related to multiphase media, which may include a continuous phase such as fluids, and a discrete phase such as powders, granular media, etc. Furthermore, these phases can behave and interact on multiple scales. The engineering applications involving such complexities are very difficult to study through experimentation. Therefore, such complex multi-physics, multi-scale problems are usually studied via numerical simulations.

2

⁴² The problems involving such mixed media, cannot be resolved well by
⁴³ only a continuous or a discrete phase alone. Such problems need to account
⁴⁴ for both continuous and discrete media along with their interactions with
⁴⁵ each other [1]. Such an approach is known as the Combined Continuum and
⁴⁶ Discrete Model (CCDM) [2]. In the present work, we will deal with the Heat
⁴⁷ and Mass Transfer (HMT) between the continuous fluid phase and discrete
⁴⁸ particles phase. HMT between fluid and particles can be used to describe
⁴⁹ processes such as drying, pyrolysis, combustion, gasification, and melting.
⁵⁰ These processes have a wide variety of applications in industrial sectors such
⁵¹ as mining, energy production, waste management, pharmaceuticals, manu-
⁵² facturing & production, and process industries. Due to the challenges in per-
⁵³ forming experiments, it is desirable to have an HMT multi-physics simulation
⁵⁴ environment between particles and fluids to better capture these phenomena.
⁵⁵ Such novel and rapidly evolving applications demand a rapid develop-
⁵⁶ ment of a simulation environment. In the literature, to achieve CFD-DEM
⁵⁷ coupling either commercial CFD software such as ANSYS Fluent®[3–8] is
⁵⁸ coupled with commercial, open-source or in-house DEM software such as
⁵⁹ Rock-DEM® [9]. Open-source software such as CFDEM (OpenFOAM +
⁶⁰ LIGGGHTS) [10] are also utilized extensively for HMT applications [11, 12].
⁶¹ The CFD-DEM couplings mentioned above are achieved by solving dif-
⁶² ferent sets of segregated equations iteratively. This is ordinarily achieved by
⁶³ a single code coupling, where all physics models are implemented in one code
⁶⁴ also known as the monolithic coupling approach. Or they are coupled using a
⁶⁵ partitioned coupling approach, that couples existing single-physics software
⁶⁶ on a high level [13].
⁶⁷ The monolithic coupling approach can be more robust when applied to
⁶⁸ specific applications. Additionally, years of extensive research and devel-
⁶⁹ opment are required to achieve such a simulation environment for a specific
⁷⁰ application. An extensive review [14] of developments in CFD-DEM coupling
⁷¹ approaches for different applications demonstrates the same. Even with these
⁷² developments, a lot more research remains to be done. However, due to the
⁷³ intrinsic nature of the monolithic coupling approach, it is rigid in its imple-
⁷⁴ mentations. Moreover, such approaches rarely allow easy modifications or
⁷⁵ adaptions to make the model closer to reality, or adapt for different applica-
⁷⁶ tions. However, the partitioned coupling approach allows such modifications
⁷⁷ or exchange of physical components.
⁷⁸ In addition to the limitations mentioned above, due to the nature of
⁷⁹ CFD-DEM coupling, the over-lapping domain (often the entire computa-

3

tional domain) is affected, and it is important to exchange the information for coupling [15]. Furthermore, these simulations are very computationally expensive. Hence, it is very important to parallelize such pieces of software. To tackle these problems a co-located partitioning strategy is proposed [15, 16]. Although this strategy solves the problems mentioned above, it also has limitations when dealing with non-conforming meshes due to the mesh/grid alignments. The unresolved CFD-DEM coupling further adds restrictions on the smallest CFD cell size, based on the largest particle size.

To circumvent the constraints of the monolithic coupling approach and offer more flexibility, we employ the preCICE coupling library [17] to develop a partitioned multi-physics simulation environment. In the partitioned coupling approach, a multi-physics problem is decomposed into multiple single physics parts and solved separately. The preCICE coupling library can be then used to couple these new or existing (highly specialized, optimized, purpose-built) single physics solvers/software to achieve the said multi-physics problem [18].

The preCICE coupling library treats these solvers/software as black-box and enables communication, and data mapping strategies. This type of coupling approach only needs nodal information from the black box. Subsequently, only standard Dirichlet and Neumann boundary conditions are applied [13].

Hence, there is no need to have access to source code, furthermore, no need to have expert knowledge of the source code of each of the solvers/software used in the partitioned multi-physics simulation. This also allows us to couple of solvers/software implemented in different languages (where currently supported languages are C++, Python, MatLAB, Fortran, and Julia). Although, to enable this communication and data mapping, a "preCICE coupling adapter" needs to be developed. Such a development requires a basic understanding of the solver/software along with its API. Hence the development of a preCICE adapter is a fairly accessible and achievable task.

The preCICE coupling library [17] and its adapters [19, 20] have been used to model Conjugate Heat Transfer (CHT) [21] between fluid and solid. Volume coupling has been utilized to simulate fracturing in a poro-elastic medium due to fluid flow [22]. Although the physical nature of coupling in this work is volumetric, the coupled system uses surface terms for equilibrium. The state-of-art on the CFD-DEM coupling is quite vast[14]. It is more useful to bring attention to the previous works using OpenFOAM and XDEM monolithic coupling [15, 23–27].

4

To rapidly establish an HMT simulations environment, our prototype couples OpenFOAM [28] with eXtended Discrete Element Method (XDEM) [1] to achieve Heat & Mass Transfer between CFD and DEM. Although either of the software mentioned can be replaced with an alternative due to the modular nature of the coupling.

Our contributions, which are novel or related to the CFD-DEM coupling strategies, are (1) a flexible partitioned CFD-DEM coupling approach achieved by (a) developing an original preCICE adapter for XDEM (first DEM preCICE adapter), (b) extending the OpenFOAM preCICE adapter [29] to enable coupling over volumetric meshes, and mass transfer; (2) the verification against monolithic coupling and validation against experimental observations of the proposed partitioned CFD-DEM coupling approach; (3) preliminary performance analysis of monolithic versus partitioned coupling approach.

The paper is organized as follows: in section 2 we present the mathematical modeling of CFD and DEM. In section 3, the partitioned coupling strategies and software development are described. In section 4, we present and compare numerical simulation results with experimental observations, these cases include heating up, drying, and pyrolysis. In section5, we compare and discuss the performance of the partitioned coupling approach with the monolithic coupling approach. Finally in section 6 we discuss the development followed by conclusions.

2. Model Description

In the following section, the governing equations for continuum fluids and discrete particles are presented. In the partitioned coupling, we couple two single-physics software, namely CFD and DEM to achieve the multiphysics CFD-DEM environment. These are presented in section 2.2 and 2.1 respectively. The partitioned coupling approach is described in the section 3. The partitioned coupling approach is compared with a legacy monolithic coupling approach. Consequently, the reader is referred to the literature for a detailed description of the XDEM + OpenFOAM legacy coupling [26, 27, 30].

2.1. Governing equations for discrete particles

XDEM predicts both the thermodynamics and dynamics of the particulate system. In the current work, the main focus will be the thermodynamics

5

153 of such particulate systems. The particle position, velocity, and acceleration
154 are computed with the *dynamics* module of the XDEM, whereas the tem-
155 perature and chemical processes are computed with the *conversion* module.

156 *2.1.1. Conversion module*

157 The conversion module of XDEM handles the heat and mass transfer
158 within the particles and between the particles. It also accounts for various
159 processes such as drying, gasification, combustion, etc. describing the inflow
160 and outflow of the gas mixture. The detailed model description of the con-
161 version module can be found in [1, 31], a summary of the governing equations
162 for the fluid present in the porous regions within particles is given below.
163 Mass conservation equation for fluids in particle pores:

$$\frac{\partial}{\partial t}(\epsilon_f \rho_f) + \vec{\nabla} \cdot (\epsilon_f \rho_f \vec{v_f}) = m'_{s,f} \tag{2.1}$$

164 where $m'_{s,f}$ is the sum of all individual species' mass production or consump-
165 tion rates due to chemical reactions, ϵ_f denotes the porosity within individual
166 particles occupied by fluid(s). The fluid species transport within this porous
167 space of the particle obeys Darcy's law:

$$-\frac{\partial p}{\partial r} = \frac{\mu_f \epsilon_f}{K}(\vec{v_f}) \tag{2.2}$$

168 One-dimensional transient energy conservation equations for particles:

$$\frac{\partial \rho c_p T}{\partial t} = \frac{1}{r_n}\frac{\partial}{\partial r}\left(r^n \lambda_{eff}\frac{\partial T}{\partial r}\right) - r^n\left(\vec{v}\rho_f c_{p_f}T\right) + \epsilon_f \sum_{k=1}^{l}\dot{\omega}_k H_k \tag{2.3}$$

169 The mass balance and transport equation of individual fluid species within
170 the particle pores:

$$\frac{\partial}{\partial t}(\epsilon_f \rho_{f,i}) + \nabla \cdot (\epsilon_f \rho_{f,i}\vec{v_f}) = \frac{1}{r_n}\frac{\partial}{\partial r}\left(r^n \epsilon_f D\frac{\partial \rho_{f,i}}{\partial t}\right) + m'_{s,f,i} \tag{2.4}$$

171 The following boundary conditions apply to the governing equations men-
172 tioned above:

$$-\lambda_{eff}\frac{\partial T}{\partial r}\bigg|_{r=0} = 0 \tag{2.5}$$

173

$$-\lambda_{eff}\frac{\partial T}{\partial r}\bigg|_{r=R} = \alpha(T_R - T_\infty) + q''_{rad} + q''_{cond} \tag{2.6}$$

6

$$-D_{i,eff} \left.\frac{\partial \rho_i}{\partial r}\right|_{r=R} = \beta_i \left(\rho_{i,R} - \rho_{i,\infty}\right) \qquad (2.7)$$

₁₇₅ In the Eq 2.6, q''_{cond} and q''_{rad} are conduction and radiation heat sources
₁₇₆ respectively from the neighboring particles. A detailed description of the
₁₇₇ conduction and radiation between particles is given by B. Peters in [31].

₁₇₈ To solve for heat & mass transfer within the particle, the particle radius
₁₇₉ is discretized. This radial discretization can be uniform or non-uniform, as
₁₈₀ shown in fig 1. In the present work, uniform radial discretization is used. The
₁₈₁ non-uniform radial discretization allows for having a smaller cell length near
₁₈₂ the particle surface that allows the model to capture the sharp temperature
₁₈₃ and mass flow gradients.

(a) Uniform discretization   (b) Non-Uniform discretization
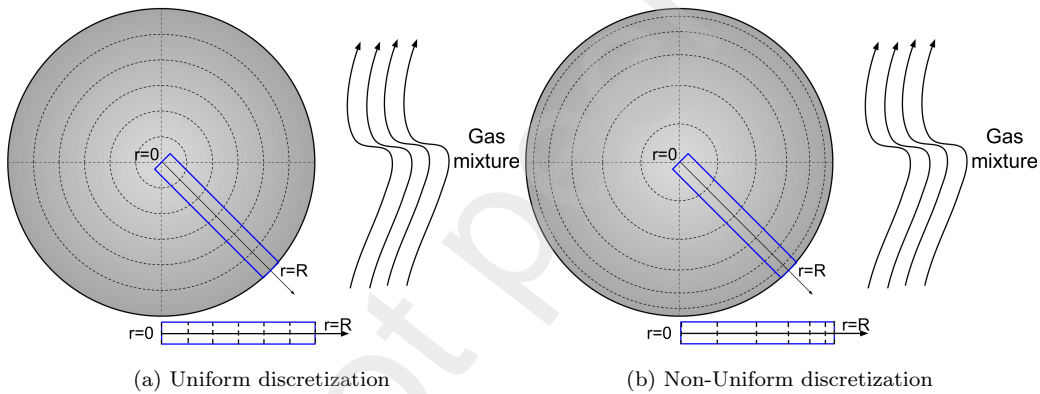
Figure 1: Radial discretization for heat & mass transfer calculations within a particle

₁₈₄ *2.1.2. Dynamics module*

₁₈₅ The discrete element method used in the dynamics module of XDEM
₁₈₆ is based on the soft sphere model. In this method, it is assumed that the
₁₈₇ particles are deformable and can overlap each other, where the magnitude of
₁₈₈ overlap is decided by the contact force using the force-displacement law. The
₁₈₉ hardness of the particle is expressed via Young's Modulus, while the particle
₁₉₀ energy dissipation is described with a dampener and/or dashpot. The trans-
₁₉₁ lational and rotational movements of individual particles are tracked using
₁₉₂ classical mechanics equations. A detailed description can be found in [23].

₁₉₃ The scope of the present work is heat and mass transfer, hence the cases
₁₉₄ chosen for this study do not have particle(s) in motion. However, if the fluid

7

195 velocities were to be increased, particles could move due to the momentum
196 transfer. The fluid velocity is modeled as one of the external forces F_i^{ext}. An
197 example of such a case can be found in the modeling of a raceway zone in a
198 blast furnace [32].

199 A summary of the translational and rotational motion equations is given
200 below:

201 Equations of particle motion, where $\vec{F_i^{ext}}$ is the sum of all the external forces
202 acting on the particle, such as buoyancy forces $\vec{F_B}$ and drag forces $\vec{F_D}$:

$$m_i \frac{d\vec{v_i}}{dt} = m_i \frac{d^2 \vec{X_i}}{dt^2} = \vec{F_i^c} + \vec{F_i^g} + F_i^{\vec{ext}} \tag{2.8}$$

203

$$I_i \frac{d\vec{\omega_i}}{dt} = \sum_{j=1}^{n} \vec{M_{i,j}} \tag{2.9}$$

204 *2.2. Governing equations for fluid*

205 In the Eulerian volumetric average method, the conservation equation of
206 mass (Eq 2.10), momentum (Eq 2.11) and energy (Eq 2.12) are written over
207 a representative volume.

208 Conservation of mass:

$$\frac{\partial}{\partial t} (\rho_f) + \nabla \cdot (\rho_f \vec{v_f}) = m' \tag{2.10}$$

209 Conservation of momentum:

$$\frac{\partial}{\partial t} (\rho_f \vec{v_f}) + \nabla \cdot (\rho_f \vec{v_f} \vec{v_f}) = -\nabla p + \rho_f \vec{g} + \mu \nabla^2 \vec{v_f} + \vec{S} \tag{2.11}$$

210 Conservation of energy:

$$\frac{\partial}{\partial t} (\rho_f h_f) + \nabla \cdot (\rho_f \vec{v_f} h_f) = \frac{\partial p}{\partial t} + \vec{v_f} \cdot \nabla p + q' \tag{2.12}$$

211 Mass conservation equation for chemical species i in CFD is given as
212 follows in Eq 2.13

$$\frac{\partial}{\partial t} \rho_{f,i} + \nabla \cdot (\rho_{f,i} \cdot \vec{v_f}) = m_i' \tag{2.13}$$

213 In the XDEM + OpenFOAM legacy coupling [26, 27, 30], the governing equa-
214 tions of the fluid contain a term ϵ (porosity), where porosity (ϵ Eq 2.14)refers

8

215 to the interstitial space between the solid particles. The porosity calculation
216 in brief is as follows:

$$\epsilon = 1 - \frac{1}{V_c} \sum_i^n \eta_i V_i \tag{2.14}$$

217 where V_c is the volume of the cell in consideration, V_i is the volume of each
218 particle multiplied by η_i denoting the amount of particle volume present in
219 the current volume.

220 This porosity term is not directly included in the current CFD model, as
221 the fluid solver needs to be modified and tested thoroughly. This process is
222 highly intrusive and defeats the rapid development of the HMT simulation
223 environment.

224 Thus when computing the heat and mass source terms in the XDEM, the
225 porosity is taken into account. Furthermore, this porosity is exchanged as a
226 field. Subsequently, it is used to model the drag offered by the particles to
227 the fluid as follows [33]:

$$\kappa = \frac{d_{p_{mean}}^2 \epsilon^3}{150(1 - \epsilon^2)} \tag{2.15}$$

228 where $d_{p_{mean}}$ is the mean particle diameter.

$$C = \frac{1.75(1 - \epsilon)}{d_{p_{mean}} \epsilon^3} \tag{2.16}$$

229

$$drag = \frac{\mu}{\kappa} + \rho C \vec{v}_f \epsilon \tag{2.17}$$

230 3. Partitioned Coupling Implementation with preCICE

231 A flexible multi-physics simulation environment is achieved through the
232 preCICE coupling library due to its minimal invasion of the solvers through
233 the usage of high-level API (Application Programming Interface). This in-
234 tegration of preCICE into the solver is known as an "adapter" [34], seen in
235 a schematic in figure 2. For a well-developed in-house, open-source, or any
236 other kind of solver, an API for the solver is generally available. Alterna-
237 tively, solvers developed in-house are well understood and can be developed
238 to facilitate data field communication through preCICE. By utilizing the API
239 from the solver and preCICE, the solver code remains unchanged, and the
240 adapter can be easily implemented and compiled as a separate library called
241 by the solver during runtime. During coupled simulation, the solver passes

9

₂₄₂ the required data via its adapter to preCICE, which in turn communicates it
₂₄₃ to the other coupled solver(s) using MPI messages or TCP/IP sockets. A list
₂₄₄ of data fields exchanged for the HMT CFD-DEM coupling for the current
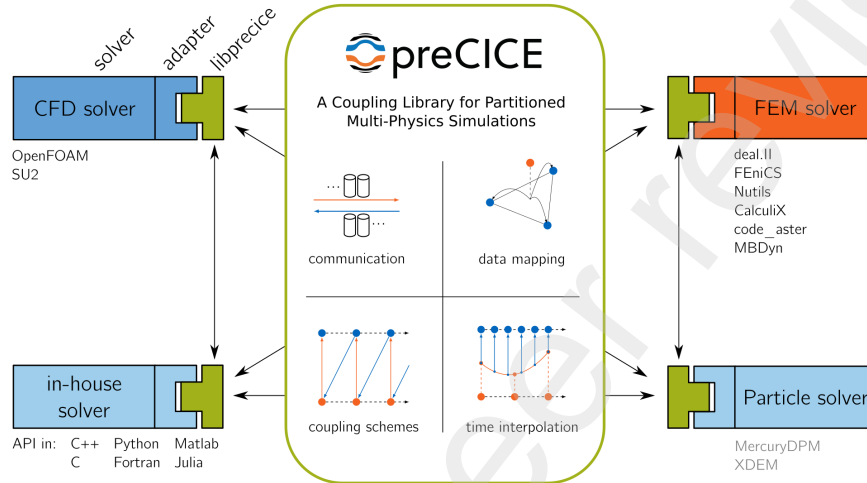₂₄₅ work is presented in table 1.

Figure 2: A schematic outlining the coupling procedure [18] (reproduced with permission)

3.1. OpenFOAM Adapter for preCICE coupling

₂₄₇   The OpenFOAM adapter [29] is already available for surface coupling.
₂₄₈ It is used in different examples and applications such as Conjugate Heat
₂₄₉ Transfer (CHT) and Fluid-Structure Interactions (FSI) that can be achieved
₂₅₀ when coupled with other software. Although the default adapter contains
₂₅₁ all the fluid fields required to achieve HMT between CFD-DEM, they are
₂₅₂ described on surfaces.

₂₅₃   To enable CFD-DEM volume coupling, a new coupling interface is imple-
₂₅₄ mented in the OpenFOAM adapter. Four different modules are implemented.
₂₅₅ These modules enable an exchange of different data fields related to Fluid
₂₅₆ Properties, Momentum Transfer, Heat Transfer (HT), and Mass Transfer
₂₅₇ (MT). Depending on the type of simulation these modules can be switched
₂₅₈ on or off (similar to the pre-existing modules).

₂₅₉   Data fields such as fluid density, viscosity, thermal conductivity, and spe-
₂₆₀ cific heat are added to the Fluid properties module. The fluid temperature
₂₆₁ and heat source fields are added to the HT module, whereas chemical species
₂₆₂ mass fractions, mass source, and species mass source are added to the MT

10

263 module. Fluid velocity and pressure fields are exchanged via the Momentum
264 transfer module. The user is free to select which data fields they want to ex-
265 change, and what modules to use. Depending on the simulation type, these
266 data fields are communicated via preCICE and the adapters to the other
267 solver(s) and make them available for calculation.

268 In addition, OpenFOAM adapter receives various source fields such as
269 heat (q'), mass (m'), and species (m'_i) through their respective modules.
270 These source fields are then injected into the respective governing equations
271 through the finite volume plugin `fvOptions` of OpenFOAM. As the presence
272 of particles in the fluid is only represented by source terms in the finite
273 volume options, there is no need to modify any of the OpenFOAM solvers to
274 accommodate this CFD-DEM coupling. In the present work, `rhoPimpleFoam`
275 (HT) and `reactingFoam` (HT & MT) solvers provided by OpenFOAM are
276 used.

277 In practice, when using OpenFOAM, one only needs to change the CFD
278 solver name in `controlDict`. If this solver has the fields required as men-
279 tioned in table 1, no more work is required to run a CFD-DEM multi-physics
280 simulation. In broad scope, it is also possible to switch between differ-
281 ent OpenFOAM versions seamlessly to avail of different functionalities and
282 solvers. With some more effort, one can also implement an adapter for an
283 in-house CFD solver, and couple it with the needed solver (XDEM in this
284 case).

285 *3.2. XDEM Adapter for preCICE coupling*

286 Similar to preCICE, XDEM is also implemented in C++, thus when
287 implementing the XDEM adapter for preCICE, we utilize C++ API of pre-
288 CICE. An XDEM coupling interface class is implemented and then utilized
289 to access data fields from the XDEM adapter.

290 XDEM adapter is developed to be flexible for diverse types of simula-
291 tion. Similar to some other preCICE adapters provided by preCICE, the
292 XDEM adapter is developed so that one can choose what fields are to be
293 exchanged. If required fluid fields are not exchanged, default values are used
294 for required calculations. XDEM adapter provides a summary of the data
295 fields exchanged and possible types of simulation being run based on the data
296 fields used. XDEM adapter receives several fields describing fluid properties
297 and flow conditions. These values are then used as boundary conditions on
298 the particles. In the context of current work, XDEM offers several HT laws
299 and MT laws [35–38]. These are set through the XDEM input file. These

11

Data Fields	CFD →DEM	DEM →CFD
Fluid Temperature	✓	
Fluid Viscosity	✓	
Fluid Conductivity	✓	
Fluid Specific Heat	✓	
H_2O	✓	
O_2	✓	
N_2	✓	
⋮	✓	
species n	✓	
Heat Source (q')		✓
Mass Source (m')		✓
Heat Transfer Coefficient		✓
Volume Porosity (ϵ)		✓
source H_2O (m'_{H_2O})		✓
source O_2 (m'_{O_2})		✓
source N_2 (m'_{N_2})		✓
⋮		✓
source species n (m'_n)		✓

Table 1: The data fields that are exchanged for the heat and mass transfer coupling

HT and MT laws are then utilized to compute the heat, mass, and chemi-
cal species source terms. Depending on the species mass concentrations and
fluid flow conditions. XDEM also performs species transport and Solid-Fluid
reactions.

These source terms are then transferred to the CFD solver through pre-
CICE. The XDEM coupling interface class and the XDEM adapter are de-
signed in such a way that ideally we can switch between any desired CFD
solver/software. It does not make an assumption the kind of CFD solver
used, rather it just assumes it receives and sends some specific fields that can
be configured. Thus providing flexibility in choosing a CFD solver based on
the application.

3.3. Mapping methods over Volumetric mesh

In the current work, we achieve the HMT coupling over volumetric meshes.
Normally, we already have a volumetric mesh for the CFD. In contrast, DEM

12

₃₁₄ is a mesh-less method. In the XDEM suite, the DEM simulation domain is
₃₁₅ defined by a simple box, and individual particles are tracked within this box.
₃₁₆ An example of such a domain can be seen in figure 15 (b). However, due to
₃₁₇ DEM methods being costly, they require some parallelization. To this end,
₃₁₈ the simple box in the XDEM suite can be discretized over the three axes.
₃₁₉ Figure 16 (b) shows the DEM domain discretized. The domain is sliced to
₃₂₀ reveal the cells and cell-centres. Consequently, the CFD cell size does not
₃₂₁ depend on the largest particle diameter for the unresolved coupling presented
₃₂₂ in this work.

₃₂₃ The numerical experiments presented to use the default mapping of-
₃₂₄ fered by the preCICE coupling library. The `nearest projection` map-
₃₂₅ ping method is applied when mapping data from CFD to DEM. In con-
₃₂₆ trast, `nearest neighbor` mapping method is applied when mapping data
₃₂₇ from DEM to CFD. The `nearest-projection` mapping method is mostly
₃₂₈ a second-order method. This method first projects the data onto the mesh
₃₂₉ and uses linear interpolation within each element [39]. An illustration of this
₃₃₀ method can be seen in the top half of figure 3. This method requires the
₃₃₁ mesh connectivity information. The `nearest neighbor` mapping method
₃₃₂ is a first-order method as presented in the lower half of the figure 3. The
₃₃₃ cases under consideration do not warrant complex mapping methods such as
₃₃₄ `nearest neighbor gradient` or `radial basis function`. Although these
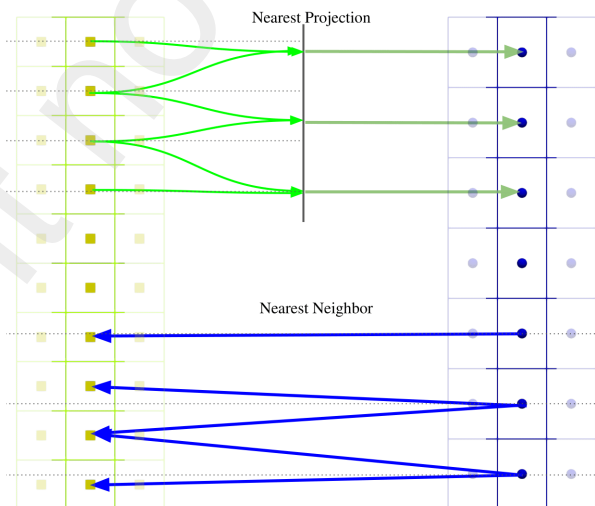₃₃₅ mapping methods are available in the preCICE coupling library.

Figure 3: A schematic showing the two data mapping strategies used

13

Further, the mappings have two different types of constraints so as to ac-
count for mapping between non-conforming meshes. These are `consistent`
and `conservative` [39]. The `conservative` mapping constraint aggregates
the data to be mapped such that the total amount of data coupled is the
same on the two meshes. In the present work, we apply the `conservative`
mapping constraint when mapping data from DEM to CFD. This ensures
that the exactly same amount of heat, mass, and/or species source generated
by the particles is injected into the CFD domain. Although, one has to be
careful with non-conforming meshes. More discussions on how this mapping
constraint affects the simulation results are in sections 4.4.1 and 6. The
`consistent` mapping constraint is applied when mapping data from CFD
to DEM. This constraint is applied for physical quantities such as tempera-
ture or velocities. This mapping constraint will apply the exact value seen
on the originating mesh. In the applications under consideration, this map-
ping constraint can be very useful as the CFD-DEM coupling is unresolved.
Depending on the mesh size differences, it can be enough to know the fluid
conditions corresponding to the CFD cell center closest to the particle center.

This constraint can be quite limiting if the mesh size difference between
CFD and DEM is large. This mapping constraint can also be limited if we
see large gradients in physical values over a distance shorter than particle
diameter. These limitations can be counteracted by employing the `radial`
`basis function` mapping instead of either methods mentioned above. Al-
though this method will give more accurate mapping and, thus more accurate
simulation results, this method is more costly. In the current work, the CFD
and DEM cell size disparity is almost non-existent (for single particle cases)
or very minor (for packed bed case).

3.4. Coupling Strategies

It is very important to consider the type of coupling needed for a given
problem. A further restriction of the monolithic coupling approaches is that
the application hence the type of coupling strategies are predefined. This can
lead to two issues, either the coupling strategy used is okay but might lead
to additional costs or the coupling strategy is ill-suited for a new problem.

In this section, we briefly discuss the coupling strategies available for
the presented partitioned coupling. There are two main distinct coupling
strategies available for partitioned coupling approaches, broadly known as
explicit and implicit. The explicit coupling strategy executes and calls the
coupled solvers for a set number of coupling time steps, whereas the implicit

14

³⁷³ coupling strategy is used when either the numerical solution is unstable or
³⁷⁴ there is a need to completely capture the coupled solution. The reader is
³⁷⁵ referred to the literature for in-depth reading [13, 39]. In the numerical
³⁷⁶ experiments presented in the next sections, we only use the explicit coupling
³⁷⁷ strategy. However, using the implicit coupling strategies could be used just
³⁷⁸ as easily without any additional work.

³⁷⁹ *3.5. Execution Strategies*

³⁸⁰   Although parallelization and scalability are not the primary focus of this
³⁸¹ work, due to the computational costs involved in discrete methods, this issue
³⁸² is bound to come up. The current partitioned coupling approaches allow for
³⁸³ the rapid development of heat and mass transfer simulation environments.
³⁸⁴ Although this might allow to establish a multi-physics simulation environ-
³⁸⁵ ment required for a certain application, it is also important that it is scalable
³⁸⁶ for the intended application. These simulations can be quite large when
³⁸⁷ considering industrial scale applications.

³⁸⁸   In the classical monolithic coupling approach, each set of equations de-
³⁸⁹ scribing one of the physics involved is executed consecutively or serially.
³⁹⁰ These equations might be parallelized, but their execution is serial. This
³⁹¹ leads to the computing resources being idle. The different execution strate-
³⁹² gies are illustrated in figure 4. Figure 4 (a) and (b) illustrates respectively the
³⁹³ execution of the monolithic coupling and the serial execution of partitioned
³⁹⁴ solvers. In terms of solving the equations, they tend to behave similar to
³⁹⁵ each other. However, in our monolithic approach, the two physics are cou-
³⁹⁶ pled into a single executable, they share the data on the memory, that is used
³⁹⁷ to exchange the information between the solvers. On the contrary, for the
³⁹⁸ partitioned execution, the exchange of data is handled through the preCICE
³⁹⁹ coupling library leading to extra memory copies and communications.

⁴⁰⁰   Figure 4 (a) and (b), in terms of the execution, there is not much difference
⁴⁰¹ apart from the way the information is shared. The big difference comes in
⁴⁰² the parallelization of individual solvers. In the monolithic approach, as the
⁴⁰³ equations are intermingled, the domain needs to be divided exactly the same
⁴⁰⁴ way for both the solvers, hence the co-located partitioning approach [16]. In
⁴⁰⁵ contrast, for the partitioned coupling approach, the domains for each solver
⁴⁰⁶ can be divided as the need arises. This feature plays an important role when
⁴⁰⁷ there are non-conforming domains/meshes involved in the coupling, which is
⁴⁰⁸ the case for most real-world applications.

15

₄₀₉ Furthermore, figure 4 (a) and (b) demonstrates another fatal flaw of this
₄₁₀ type of execution, i.e. wasting computing resources by idling. As the solvers
₄₁₁ execute one after the other, one solver always has to wait for the other solver
₄₁₂ to finish. Consequently, a parallel execution strategy can be utilized to avoid
₄₁₃ this problem, as illustrated in figure 4 (c). Here, both solvers are executed
₄₁₄ simultaneously. In this example, we see that the DEM solver requires more
₄₁₅ time, hence the CFD solver computing resources stay idle, but the overall
₄₁₆ idle time as compared to the serial execution is less. This problem of idling
₄₁₇ can also be solved by further load balancing.

4. Results

₄₁₉ In the present work, we use simple fundamental test cases to demonstrate
₄₂₀ the robustness of the partitioned HMT coupling between CFD and DEM.
₄₂₁ Along with the simple cases, we also study the drying process of a packed
₄₂₂ bed [40] to demonstrate the coupling with a large number of particles. To
₄₂₃ validate and verify the coupling, we compare the simulation results from
₄₂₄ the current coupling methodology with experimental results and simulation
₄₂₅ results from legacy CFD-DEM (XDEM). The current work only focuses on
₄₂₆ convective heat transfer between particles and fluid, as inter-particle heat
₄₂₇ transfer has been extensively studied in previous work [30, 33].Conduction
₄₂₈ and radiation between particles and fluid can also be modeled similarly, but
₄₂₉ for the current cases their contribution is insignificant, hence we ignore these
₄₃₀ heat sources.

₄₃₁ The XDEM + OpenFOAM preCICE coupling uses OpenFOAM v7 [28].
₄₃₂ However, XDEM + OpenFOAM legacy coupling uses FOAM-Extend v3.2 [41],
₄₃₃ which is a fork of OpenFOAM. This different implementation might lead to
₄₃₄ minor numerical differences in the results. The software used for legacy
₄₃₅ coupling are a modified version of foam-extend 3.2 (git hash $3912d19b$) and
₄₃₆ XDEM (git hash $fd06b8a0$). The preCICE coupling uses OpenFOAM 7,
₄₃₇ XDEM (git hash $a6f0b7f9$) and preCICE 2.5.0. The simulations are carried
₄₃₈ out on the *Aion* cluster at the University of Luxembourg that offers 354 com-
₄₃₉ puting nodes, consisting of two AMD Epyc ROME 7H12 2.6Ghz processors
₄₄₀ accounting for 128 cores per computing node, each equipped with 256 GB of
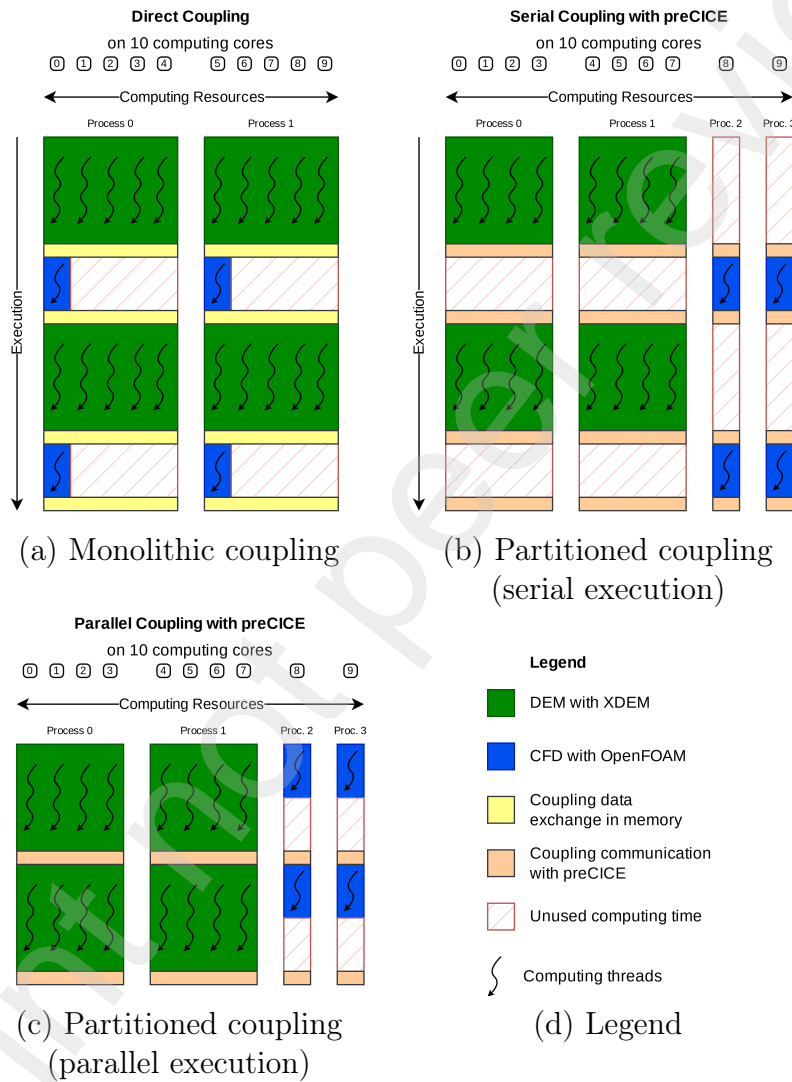₄₄₁ memory.

16

(a) Monolithic coupling

(b) Partitioned coupling (serial execution)

(c) Partitioned coupling (parallel execution)

(d) Legend

Figure 4: Comparison of the coupling and execution strategies

This preprint research paper has not been peer reviewed. Electronic copy available at: https://ssrn.com/abstract=4668107
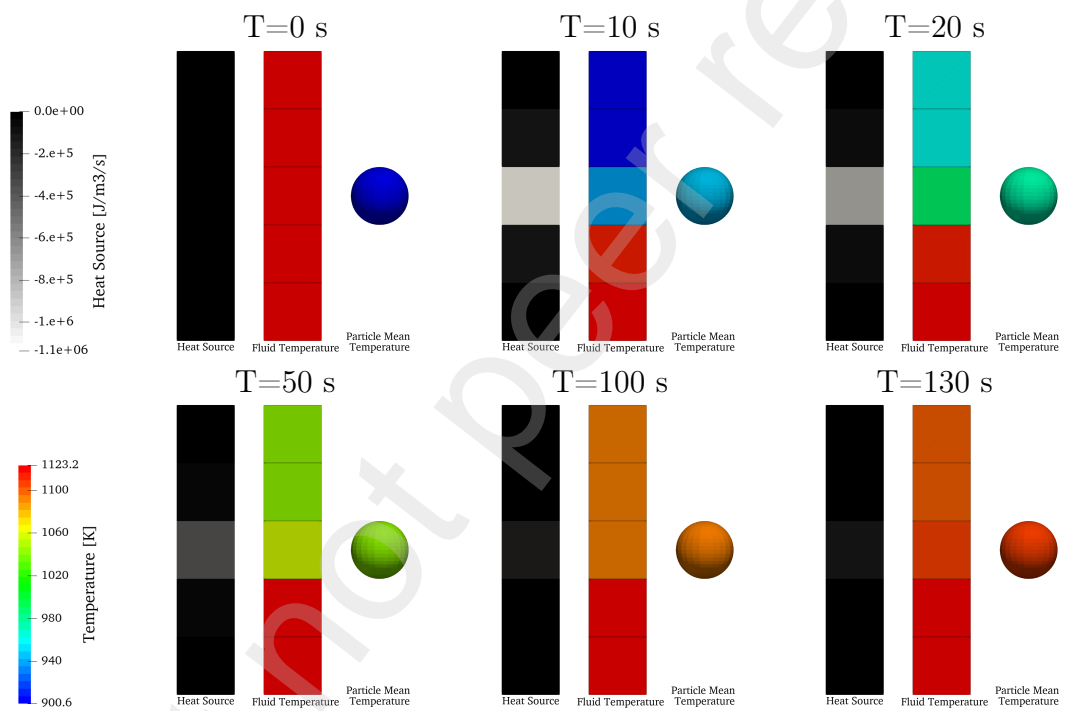
Figure 5: Fluid fields demonstrate the effect of the presence of cold particle heating-up

18

4.1. Heat Transfer only: Single particle heat-up

443 In the heat transfer only case, we consider one particle at room temper-
444 ature heating up due to the hot air surrounding it. The CFD domain is
445 $0.02 \times 0.02 \times 0.1$ m in size, discretized into 5 cells in the vertical direction
446 only (uniform 3D Grid $1 \times 1 \times 5$). The air inside the fluid domain is at 1123
447 K and atmospheric pressure is $1e + 05$ Pa. The air enters from the bottom
448 of the CFD domain with 0.38 m/s and a temperature of 1123 K, mimicking
449 the experimental setup in [42]. The air exits the CFD domain from the top.
450 The DEM domain contains a dry spherical Beech wood particle of di-
451 ameter 0.02 m, with wood properties found in Table 2 [25]. The particle
452 is discretized radially into 30 uniform segments for 1D HMT computations
453 within the particle. The particle is at 300 K at the beginning of the simula-
454 tion. The particle is located at $(0.01, 0.01, 0.05)$ m and it remains stationary
455 throughout the simulation.

Properties	Beech wood [40]	Fir wood [43]
Density ρ (kg/m^3)	750	330
Porosity ϵ (-)	0.64	0.6
Pore diameter	50×10^{-6}	50×10^{-6}
Specific Heat c_p (J/kg K)	2551.3	1733
Conductivity λ (W/m K)	0.47	0.2

Table 2: Physical properties of the wood particles

456 *4.1.1. Heat transfer case results*

457 Figure 5, we see the temporal evolution of the CFD domain and particle
458 surface temperature. Figure 5 and 6 show that the particle uses thermal
459 energy from fluid to heat up. This drain of thermal energy leads to a drop
460 in the air temperature downwind. As the particle heats up, the rate of heat
461 transfer drops, and we see that the air temperature downwind gradually
462 increases, although it remains somewhere between the CFD inlet temperature
463 and the particle surface temperature. From figure 6, we see that the particle
464 surface temperature comes close to the fluid temperature. These results
465 demonstrate how two-way HMT coupling works, as we see the effects of
466 fluid conditions on the particle and the effect of the particle on the fluid

19

467 temperature field. Figure 6 also shows the drop in fluid outlet temperature.
468 The sudden initial drop-off in fluid outlet temperature is because the results
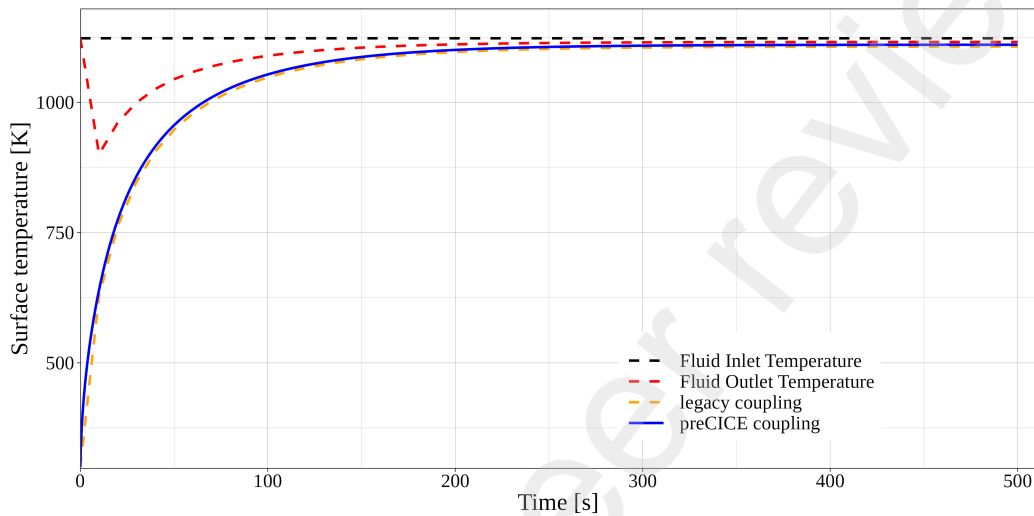**469** for fluid are recorded every 10 s, starting at 10 s.

Figure 6: Influence on fluid temperature due to the presence of particle plotted along with the surface temperature of the particle

470   Figure 6 and 7 show the particle surface and center temperature evolution
471 over time. The current results are compared with the XDEM-OpenFOAM
472 legacy coupling which has been thoroughly verified and validated against ex-
473 perimental results. Figure 6 and 7 shows that the temperature evolution of
474 the particle for XDEM + OpenFOAM preCICE coupling is in good agree-
475 ment with XDEM + OpenFOAM legacy coupling.
476   We can see that the temperature profile is in very good agreement, but
477 we see a minor difference in the numerical results. This is because we use
478 different OpenFOAM versions.
479   Figure 6 and 7 shows that the XDEM + OpenFOAM preCICE coupling
480 simulation results, specifically the particle surface and particle center tem-
481 peratures are in good agreement.
482   As there is no experimental data for the heating up of a single wood par-
483 ticle, we use the experimental results by Petek [42]. The simulation setup
484 mimics the experimental setup, the only difference being the current case
485 does not simulate any chemical reactions (pyrolysis). In figure 8, the sim-
486 ulated surface temperature of the particle closely follows the experimental

20
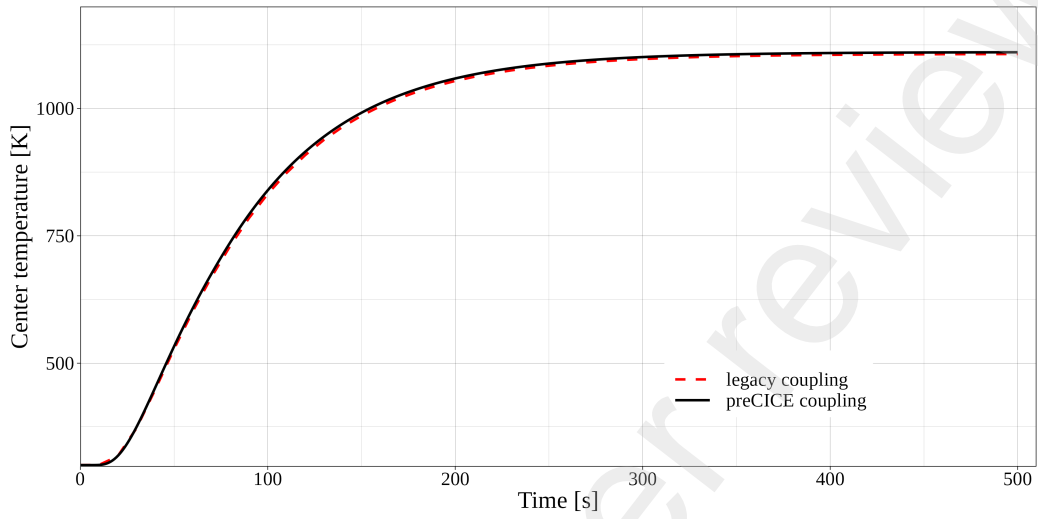
Figure 7: Temperature at the center of the particle compared for two different couplings
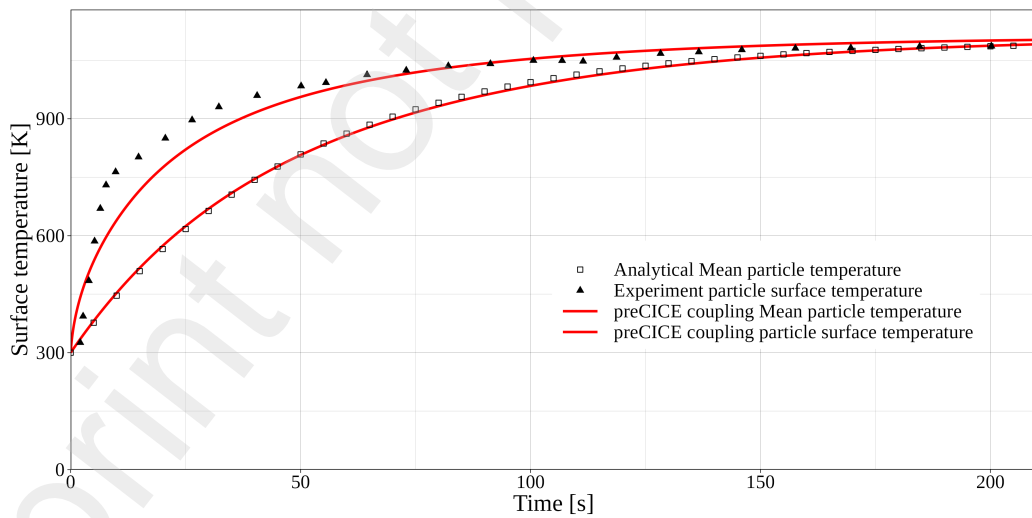
Figure 8: Particle surface and mean temperatures compared against experimental observations [42] and analytical solution resp.

21

observations. This is expected as the majority of the chemical reactions are taking place within the particle as compared to on the particle surface. In the experiment, the particle undergoes pyrolysis (an endothermic reaction), thus we see lower temperatures in the numerical simulations as compared to experimental observations for the time range 0 s & 75 s.

Furthermore, as the presented case is simple, we utilize the same initial and boundary conditions and get an analytical solution for the heat-up of the particle. As this is an analytical solution, and the particle diameter is not discretized as shown in figure 1, thus we only have the analytical solution for the overall particle temperature. The numerical result of the mean particle temperature is compared with the analytical solution in figure 8. The numerical results are in good agreement with the analytical solution.

4.2. Heat & Mass Transfer: Drying of Fir wood particle

In the previous section, we establish that the 2−way heat transfer between the CFD and DEM is working well. In the current section, we want to see the effects of this heat transfer on the composition of the particle. Particle drying is selected to validate the mass transfer as the moisture content in the particle and water vapor after evaporation stays stable, i.e. does not react with the surrounding fluid. Thus it is easy to track, in experiments as well as in simulations.

In the heat and mass transfer case, we consider drying a spherical Fir wood particle with properties given in Table 2 [43] with some moisture content. The simulation set-up conditions mimic the experimental setup by B. Peters [43]. The experiments were performed with Fir wood particles with 33% and 66% moisture content. In the current work, we perform two simulations with these two different initial moisture content. The CFD domain is $0.15 \times 0.15 \times 0.5$ m in size, discretized uniformly as $3 \times 3 \times 10$. The air inside the fluid domain is at 743 K and atmospheric pressure is $1e+05$ Pa, air enters from the bottom of the CFD domain with 0.28 m/s and a temperature of 743 K. The air exits the CFD domain from the top.

The DEM domain contains a Fir wood particle of diameter 0.008 m, located at $(0.075, 0.075, 0.125)$ m. The particle is discretized radially into 21 uniform segments for 1D HMT computations within the particle. The particle is at 297 K at the beginning of the simulation.

In the current study, the heat sink model (constant evaporation model) is applied for the calculation of drying rate [40, 43]. The model is described
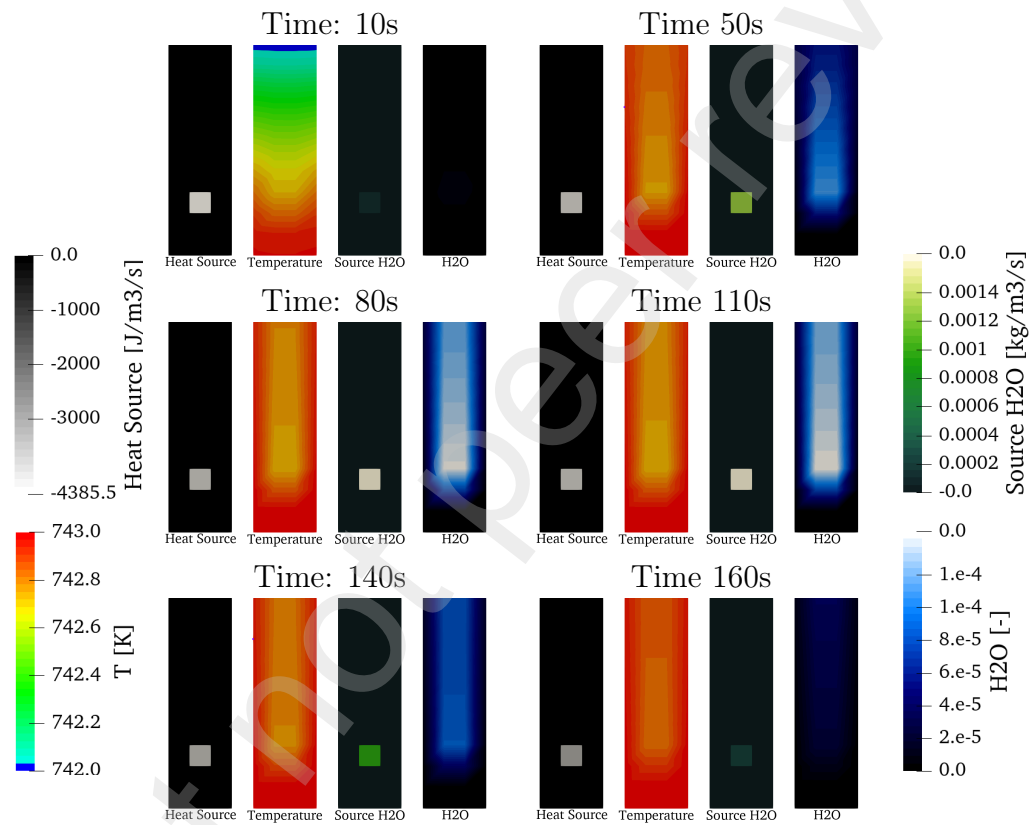
22

Figure 9: Evolution of heat source, fluid temperature, water vapor source, and water vapor mass fraction over time in the CFD domain showing drying process of wet particle.

This preprint research paper has not been peer reviewed. Electronic copy available at: https://ssrn.com/abstract=4668107

523 as follows:

$$\dot{w}_{H_2O} = \begin{cases} \frac{(T-T_{evap})\rho c_p}{H_{evap}\delta t} & \text{if } T \geq T_{evap} \\ 0 & \text{if } T \leq T_{evap} \end{cases} \tag{4.1}$$

524 where ρ and c_p are the density, and thermal capacity of the dry wood, H_{evap}
525 is the evaporation enthalpy. In this drying model, the evaporation tempera-
526 ture T_{evap} is utilized for evaporation without distinguishing between free and
527 bound water.

528 *4.2.1. Heat and mass transfer: Drying case results*

529   Figure 10 shows a comparison of the moisture content of numerical sim-
530 ulation with experimental observations for the Fir wood particle. In figure
531 10, the triangles and the circles represent the experimental results [43]. The
532 solid and small dashed lines represent the moisture content of the particle for
533 the XDEM + OpenFOAM preCICE coupling over time. Drying is described
534 as evaporation due to energy balance in conjunction with a given evapora-
535 tion temperature for the current work. We see that these simulated moisture
536 contents of the wood particle is in good agreement with the experimental
537 results. Whereas for the case with 66% initial moisture, as seen in the figure
538 10, the mean particle temperature goes beyond the water evaporation tem-
539 perature (373K at atmospheric pressure) and remains their from $\sim$ 75 s to
540 $\sim$ 175 s. Because of this we initially see comparatively lower evaporation in
541 the simulated results as compared to the experimental observations. Finally,
542 at around 175 s, the evaporation of water matches the experimental observa-
543 tions, but we see comparatively accelerated evaporation due to higher mean
544 particle temperature. Although the residual moisture mass fraction does not
545 exactly match the simulated results for the 66% initial moisture content, the
546 results are in good agreement as the overall evaporation time and profile are
547 similar.

548   We also compare the XDEM + OpenFOAM preCICE coupling to XDEM
549 + OpenFOAM legacy coupling and we see that the results are almost iden-
550 tical. In Figure 11, the mean temperature of the particle is compared for
551 the different coupling approaches. We can see that the temperature profile
552 for 33% moisture content in the particle is almost identical for the different
553 coupling methods, and the temperature profile for 66% moisture content in
554 the particle is in very good agreement for $2/3^{rd}$ of the simulated time, with
555 minor differences towards the end.

24

556 In Figure 9, we see various fluid fields at different stages of time. A
557 negative heat source is seen on the fluid side, which denotes that thermal
558 energy from the fluid is siphoned off to heat the particle. This is confirmed
559 by the drop in air temperature downstream of the particle location. As the
560 particle heats up, the thermal energy is used to evaporate the water in the
561 wood particle. This water vapor is being injected into the fluid domain. We
562 confirm the injection of water vapor from the particle into the fluid domain
563 by observing the transport and diffusion of the water vapor downstream.
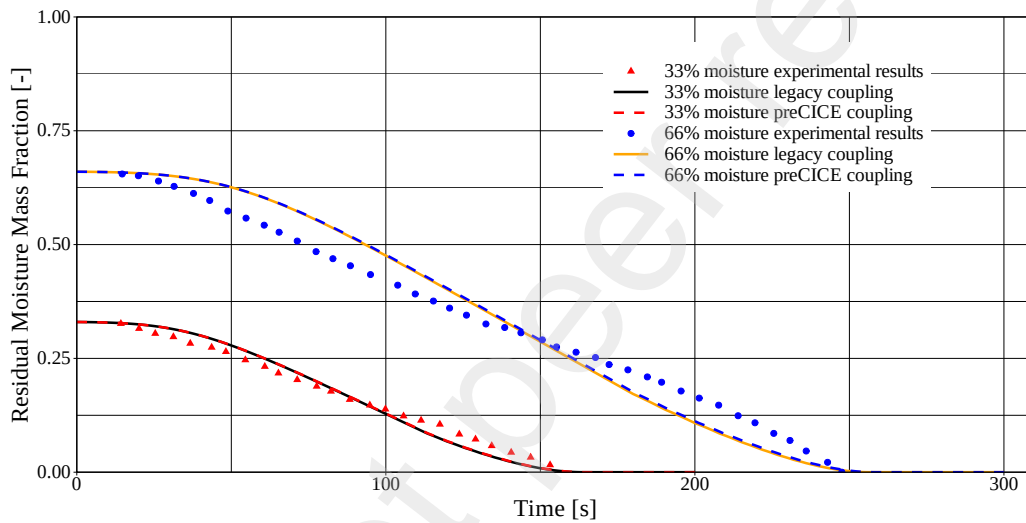
Figure 10: Particle drying simulations compared with experimental drying observations
for different initial moisture content in the particle

564 *4.3. Heat & Mass Transfer: Pyrolysis of Beechwood particle*

565 In the two previous sections, it is thoroughly established that the 2-way
566 Heat & Mass Transfer coupling between CFD and DEM works well. In the
567 previous section, where we simulate the drying process, although the particle
568 loses mass, there are no changes in the chemical composition of the particle.
569 In the current case, this is exactly what is achieved. The CFD domain is
570 $0.02 \times 0.02 \times 0.1$ m in size, discretized into 5 cells in the vertical direction
571 only (uniform 3D Grid $1 \times 1 \times 5$). The air inside the fluid domain is at
572 1123 K and atmospheric pressure is $1e + 05$ Pa. The air enters from the
573 bottom of the CFD domain with 0.38 m/s and a temperature of 1123 K,
574 mimicking the experimental setup by Petek [42]. The particle undergoes
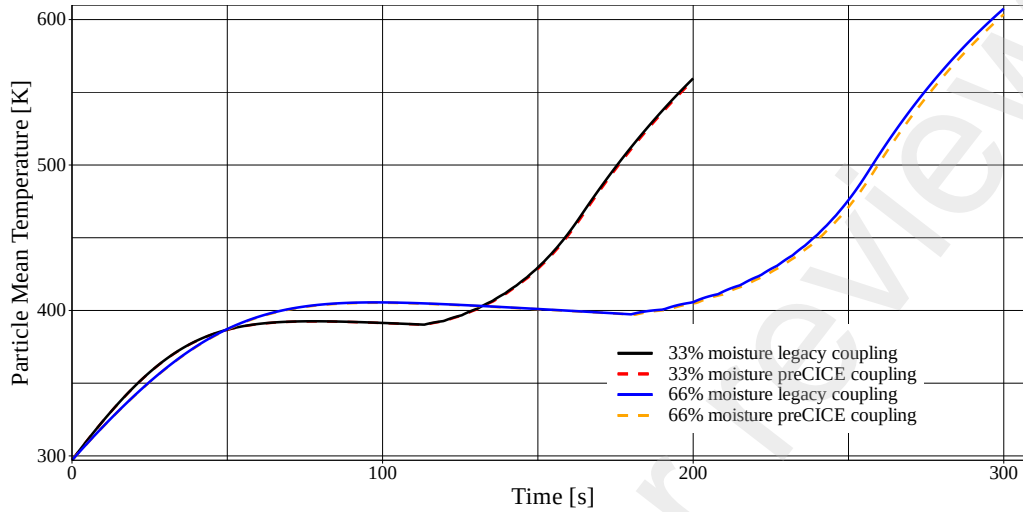
25

Figure 11: Comparison of the evolution of particle mean temperature over time for different coupling and different initial particle moisture content

⁵⁷⁵ chemical conversion described in the chemical reactions 4.2, 4.3 and 4.4. The
⁵⁷⁶ air exits the CFD domain from the top.
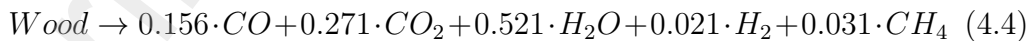
⁵⁷⁷ *4.3.1. Chemical reactions*

⁵⁷⁸ In the present work, pyrolysis of a wood particle is simulated and validated
⁵⁷⁹ against the experiments performed by Petek [42]. Pyrolysis is described with
⁵⁸⁰ three independent reactions 4.2, 4.3 and 4.4 expressing the decomposition of
⁵⁸¹ wood into its main products char, tar and gases [30].

$$Wood \rightarrow Char \tag{4.2}$$

⁵⁸²

$$Wood \rightarrow Tar \tag{4.3}$$

⁵⁸³

$$Wood \rightarrow 0.156 \cdot CO + 0.271 \cdot CO_2 + 0.521 \cdot H_2O + 0.021 \cdot H_2 + 0.031 \cdot CH_4 \tag{4.4}$$

⁵⁸⁴ *4.3.2. Heat and mass transfer: Pyrolysis case results*

⁵⁸⁵ The simulation results for particle mass loss due to pyrolysis are pre-
⁵⁸⁶ sented in figure 12 and validated against the experimental observations. The
⁵⁸⁷ predicted particle mass loss is in good agreement with the experimental obser-
⁵⁸⁸ vations. The particle surface temperature and centre temperature simulation

26
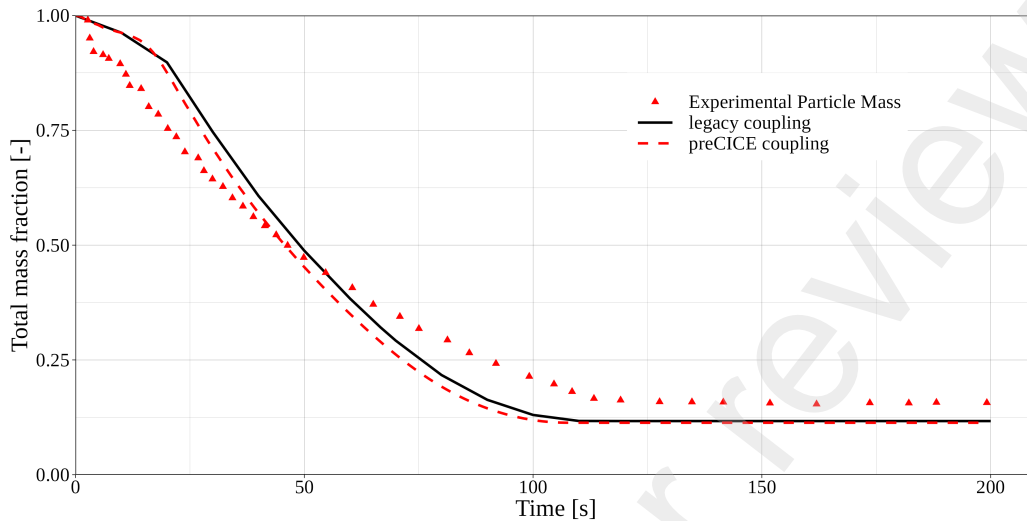
Figure 12: Comparison of the evolution of particle mass overtime for different coupling validated against experimental results of Petek [42]

results are compared with the experimental observations in figure 13 and figure 14 respectively. The predicted particle surface and center temperatures are in good agreement with the experiments.

From figure 13, it can be seen that the particle surface temperature for numerical simulation rises slowly as compared to the experimental observations, from 0 s to ∼ 80 s. The particle in the experiments experiences comparatively higher fluid velocities than the numerical simulations, as the particle in the numerical simulation, as it occupies a comparatively higher area in the fluid flow. This is because the particle in the numerical simulations is not fully resolved in the fluid domain. The two different simulations presented use two different strategies. For the XDEM+OpenFOAM legacy coupling, the CFD-DEM coupled solver is developed specifically for such applications. In this specialized solver, the particles are represented as porosity (eq 2.14). Whereas for the XDEM+OpenFOAM preCICE coupling particles are represented as source term, in this case, momentum source term. As can be seen from the figure 13, XDEM+OpenFOAM legacy coupling has a comparatively higher temperature than XDEM+OpenFOAM preCICE coupling due to the same reason mentioned above. Due to the presence of the porosity term in the fluid governing equations, legacy coupling particles experience a comparatively higher velocity than preCICE coupling.
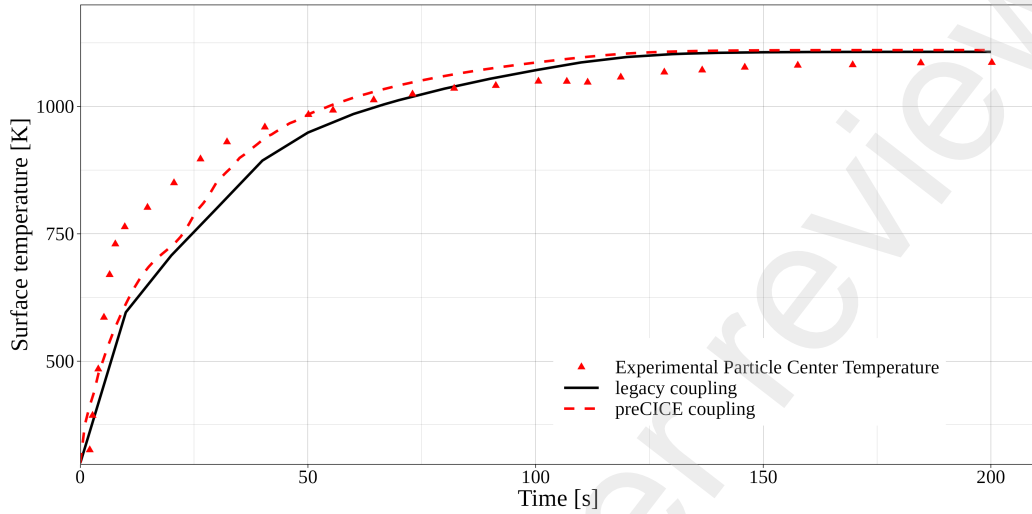
27

Figure 13: Comparison of the evolution of particle surface temperature over time for different coupling validated against experimental results of Petek [42]
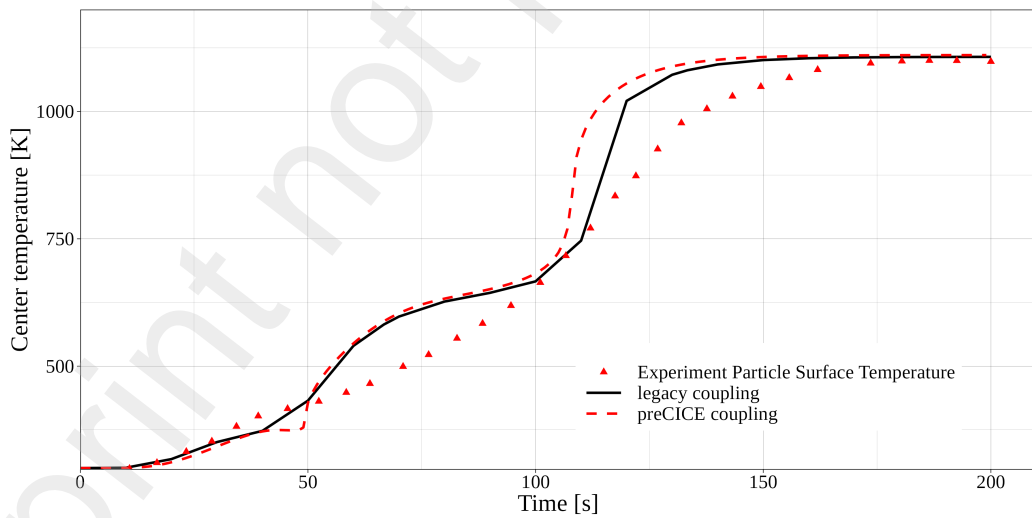

Figure 14: Comparison of the evolution of particle center temperature over time for different coupling validated against experimental results of Petek [42]

28

⁶⁰⁹ As the particle surface temperatures are higher for the legacy coupling,
⁶¹⁰ we also see a similar phenomenon for the particle center temperature in figure
⁶¹¹ 14.

⁶¹² *4.4. Heat & Mass Transfer: Drying of packed bed*

⁶¹³ The experimental data used for validation in the current case was ob-
⁶¹⁴ tained by Peters [40] on the test reactor Pantha. The reactor was set up
⁶¹⁵ to investigate heating-up, drying, and pyrolysis of packed beds. The ex-
⁶¹⁶ periments were carried out on around 2kg of air-dried $10 \times 10 \times 10$ mm^3
⁶¹⁷ cubical Beech wood containing about 10% moisture by mass. The Beech-
⁶¹⁸ wood is placed in a cylindrical bed of 250 mm diameter and 190 mm height.
⁶¹⁹ The simulation model is based on the experimental setup, a detailed descrip-
⁶²⁰ tion of the experimental setup is available in reference [40]. The experiments
⁶²¹ were performed using cubical particles, which are modeled as spheres of equal
⁶²² volume (particle radius = 6.2 mm). Thus the bed is filled with 2667 par-
⁶²³ ticles.The drying model described in equation 4.1 is utilized for the drying
⁶²⁴ of the packed bed. In addition to the convective heat transfer, the particles
⁶²⁵ also experience heat transfer through conduction.

⁶²⁶ The CFD simulation mesh can be seen in figure 15 (a) and the DEM
⁶²⁷ simulation domain with particles within it can be seen in the figure 15 (b). An
⁶²⁸ additional height of 80 mm and 60 mm on the top and bottom respectively.

⁶²⁹ The dimensions for the CFD domain are same as those mentioned above
⁶³⁰ for the DEM model. The air enters the CFD domain from the top of the
⁶³¹ cylindrical, with a temperature of 423 K and a velocity of 0.113 m/s. The
⁶³² air exits the CFD domain at the bottom of the cylinder.

⁶³³ In the figure 16, the CFD domain and DEM domain are presented. These
⁶³⁴ meshes are sliced to expose the cell centers that are used to exchange data.

⁶³⁵ *4.4.1. Heat and mass transfer: Drying of packed bed case results*

⁶³⁶ In the experiments [40], as the beech wood particles were heated up and
⁶³⁷ dried, they were measured at certain time intervals to measure the mass
⁶³⁸ loss. The evaporated moisture was also collected in a cold tube and weighed.
⁶³⁹ These measurements were used for the mass balance in the experiments, are
⁶⁴⁰ are to be used for validation of the current numerical simulation results.

⁶⁴¹ The particle weights in the numerical simulation are integrated for each
⁶⁴² time step, so we have one value for the mass (or mass loss) of the entire
⁶⁴³ packed bed. This is possible as we track the information for all the parti-
⁶⁴⁴ cles. Finally, in figure 17 we compare the dimensionless moisture loss from
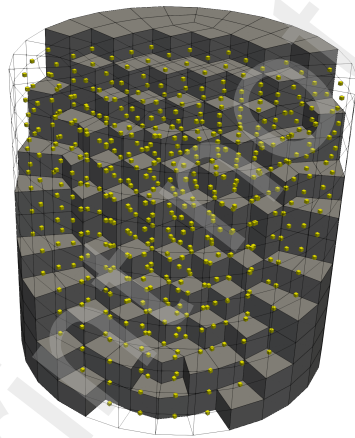
29
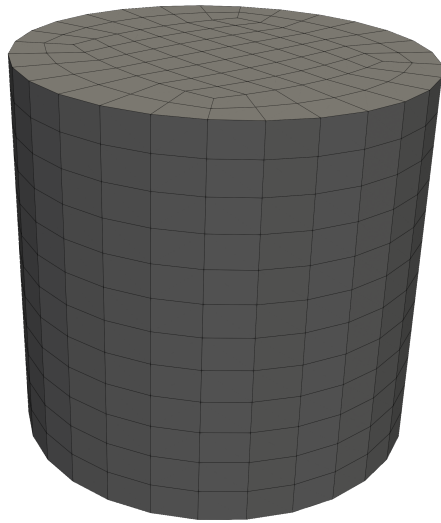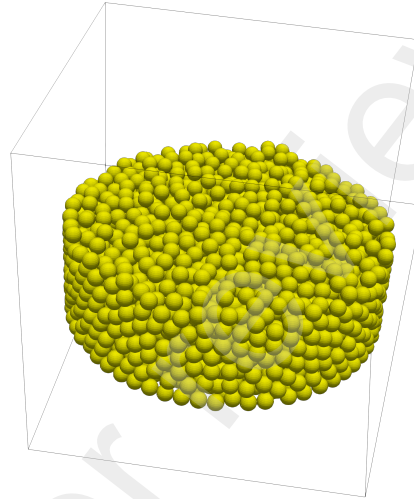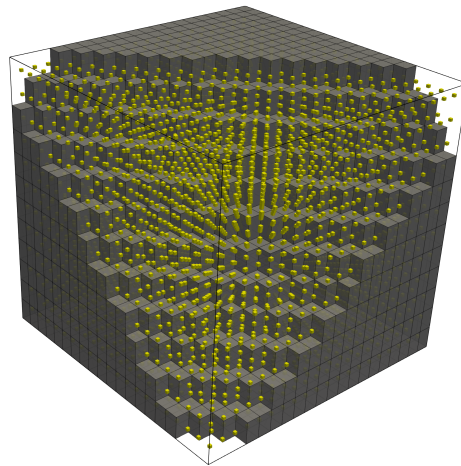
(a) CFD Mesh   (b) DEM domain with wood particles

Figure 15: Simulation model for drying of packed bed

(a) CFD Mesh   (b) DEM domain

Figure 16: CFD and DEM mesh sliced to show the cells and cell centers used for volume coupling
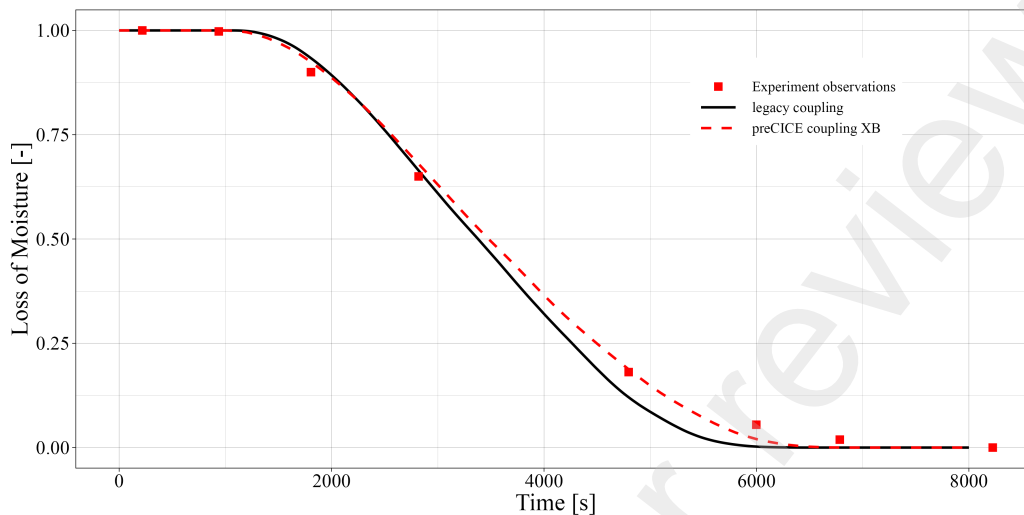
30

Figure 17: Comparison of the numerical simulation moisture content with the experimental observations

the current partitioned coupling strategy to the legacy CFD-DEM coupling as well as the experimental results. There is good agreement between the partitioned coupling approach numerical results with the experimental observations. We also see that the numerical simulation results from the current work agree with the experimental observations better as compared to the legacy coupling.

Additionally, the evolution of the moisture content (left column) and the mean temperature (right) of the packed bed is presented in figure 18 and 19 over 8000 s (same as experiment time). It is observed that the particles at the very edge start heating up more as compared to the particles in the center. Consequently, we see the drying of these particles first, as the particle temperature goes over the evaporation temperature. These initial pockets of concentrated heat in figure 18 are observed due to the `conservative` mapping constraint. This mapping constraint aggregates the heat source at the edges into the near wall, thus heating the particles at the edges faster than the centrally located particles. But as time progresses, and the particles in the pockets on the edge reach a temperature similar to fluid temperature, the rest of the bed starts heating up. This behavior is similar to that we see in the numerical results presented in the literature [26]. As the particles
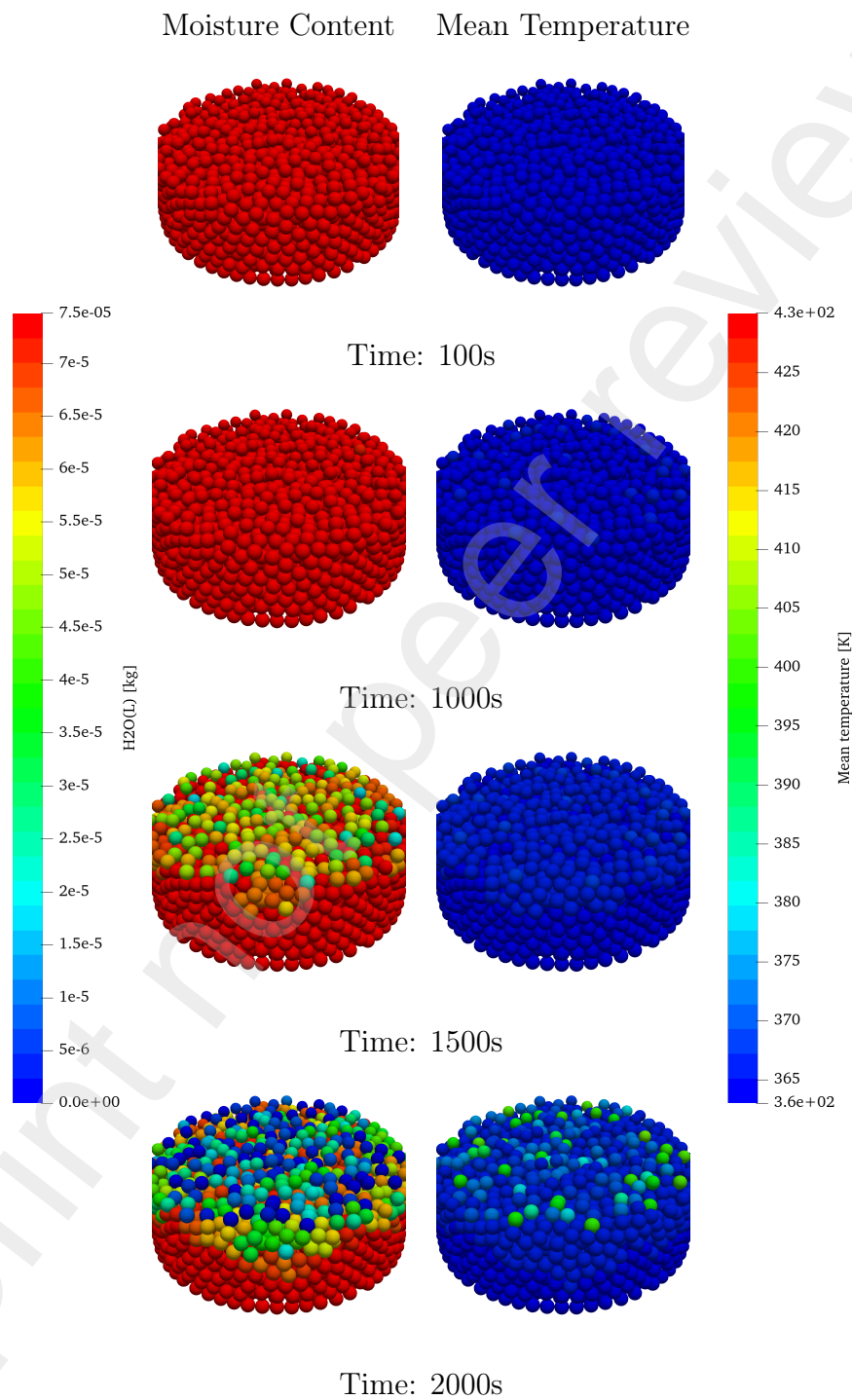
31

Moisture Content   Mean Temperature

Time: 100s

Time: 1000s

Time: 1500s

Time: 2000s

Figure 18: Evolution of particle moisture content and particle mean temperature from 100 s to 2000 s

32

Moisture Content   Mean Temperature
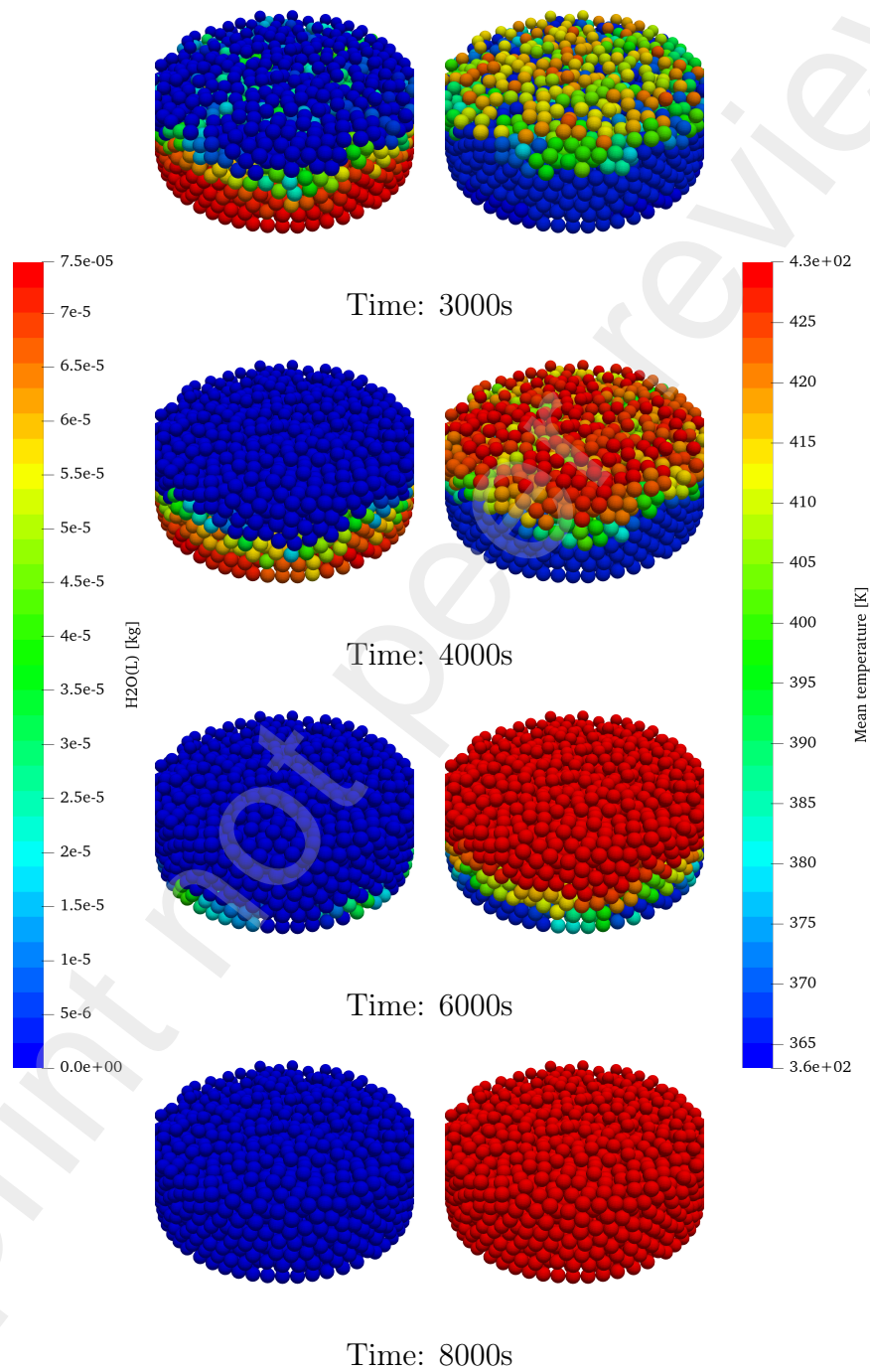
Time: 3000s

Time: 4000s

Time: 6000s

Time: 8000s

Figure 19: Evolution of particle moisture content and particle mean temperature from 2000 s to 8000 s

33

5. Performance study

The previous sections of the article sufficiently demonstrate that the CFD-DEM HMT coupling works well and the results agree with the experimental observations. Although the scope of this study is only the development and validation of the proposed partitioned coupling approach, the authors believe a brief performance study will round out the completeness and inform the reader well when choosing between monolithic and partitioned coupling approaches.

The XDEM suite allows two kinds of parallelization: coarse-grain parallelism with MPI and fine-grain parallelism with OpenMP. On their side, foam-extend and OpenFOAM only support MPI parallelization. The pre-CICE coupling library allows different coupling strategies: `serial` vs `parallel` and `explicit` vs `implicit`, as explained in the section 3.5 and illustrated in the figure 4. The `serial` type of couplings refers to staggered execution of the coupled solvers. On the contrary, the `parallel` type coupling allows the coupled solvers to execute simultaneously, allowing functional parallelism. The `explicit` type of coupling only executes once per coupling time step whereas `implicit` refers to the type of coupling where the coupled solvers execute until convergence. In the present work, `serial-explicit` and `parallel-explicit` coupling schemes are utilized. To summarise, the legacy coupling implementation behaves in the same way as `serial-explicit` pre-CICE coupling, where each coupled solved is executed in a staggered way.

Furthermore, it is to be noted that the load balancing is dependent on the case and its configuration. To illustrate this point, we present a performance study for the Pantha case in its original form and the Pantha case where the number of particles and CFD cells are increased. For the performance study, we only simulate 100 s, as this is enough to get performance behavior. This is because we have a constant number of particles throughout the simulation, and they do not move.

5.1. Performance evaluation of packed bed

In the Pantha simulation case presented in section 4.4.1, the packed bed contains only 2667 particles, thus the use of a single computing node with 128 cores for XDEM is sufficient. On the CFD side, the CFD mesh is composed of 1260 cells, hence it does not warrant using parallel execution and it is executed sequentially.

34

⁶⁹⁹ In the figure 20, we compare the legacy coupling with the preCICE cou-
⁷⁰⁰ pling. The blue column in all the plots signifies the execution time needed
⁷⁰¹ for XDEM, whereas the green column represents the execution time for the
⁷⁰² OpenFOAM. As the legacy coupling is implemented as a monolithic solver,
⁷⁰³ the CFD and DEM solvers are executed one after the other. The data ex-
⁷⁰⁴ change or the coupling is done over a shared memory. Hence, we do not
⁷⁰⁵ record a separate coupling time, it is included in the XDEM execution time.
⁷⁰⁶ On the contrary, for the preCICE coupling, the execution time for XDEM,
⁷⁰⁷ OpenFOAM, and total time are recorded. The red column representing
⁷⁰⁸ preCICE contains all the time not spent on XDEM and/or OpenFOAM
⁷⁰⁹ execution. Consequently the red column representing preCICE cost, in-
⁷¹⁰ cludes data exchange, data communication through sockets/network, inter-
⁷¹¹ polation of data between meshes, mapping data, and synchronization be-
⁷¹² tween the solvers/processes. The time required for the mapping for the
⁷¹³ `serial-explicit` and `parallel-explicit` are the same. However, it should
⁷¹⁴ be noted that the synchronization time, hence the preCICE time also includes
⁷¹⁵ the time a solver is waiting for the other solver to finish and proceed.
⁷¹⁶ In the figure 20 (a), (b) and (c), the XDEM is executed using 16 OMP
⁷¹⁷ threads, whereas in the figure 20 (d), (e) and (f), XDEM is executed using
⁷¹⁸ 64 OMP threads. It is apparent from these figures that for the case under
⁷¹⁹ consideration, preCICE coupling costs are quite significant. For this case,
⁷²⁰ preCICE coupling takes almost twice as much time as required by the legacy
⁷²¹ coupling. It is to be noted that although the original case set-up remains
⁷²² identical for the two couplings, the legacy coupling uses the CFD mesh for
⁷²³ coupling (containing 1260), whereas preCICE considers both CFD mesh and
⁷²⁴ DEM domain discretized as seen in figure 16, which has 4800 cells. This issue
⁷²⁵ is addressed in the next section.
⁷²⁶ In figure 20 (c) and (f), the OpenFOAM and XDEM are executed simul-
⁷²⁷ taneously using the `parallel` coupling, hence they are plotted side-by-side.
⁷²⁸ The light colors for each solver signify the idle/waiting time for the respective
⁷²⁹ solver. It can be seen in the figure 20 (c), XDEM takes more time overall
⁷³⁰ than OpenFOAM, hence the OpenFOAM ends up waiting for XDEM. In con-
⁷³¹ trast, when we use more computing cores for XDEM, as seen in figure 20 (f),
⁷³² XDEM ends up waiting for OpenFOAM. Due to the nature of the computa-
⁷³³ tional load, we see a minor performance gain when using `preCICE-parallel`
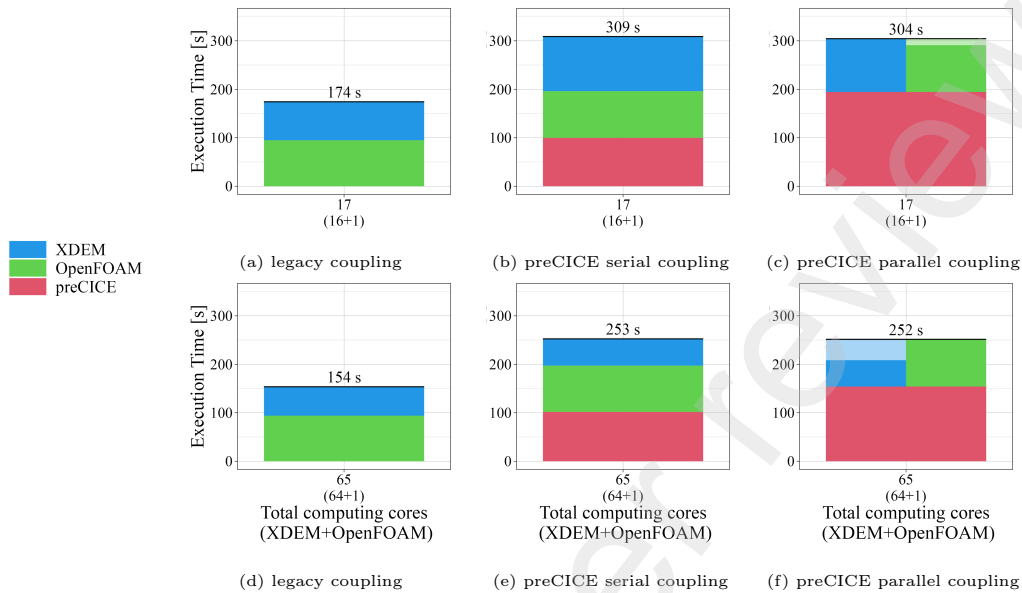⁷³⁴ as opposed to `preCICE-serial`.

35

Figure 20: Performance comparison of the Pantha case for the legacy coupling vs the preCICE serial and parallel coupling

5.2. Performance evaluation of large packed bed

Through the literature [44], it is known that load balancing for the multi-physics coupled simulations is challenging and dynamic depending on various factors. In the previous section 5.1, it seems like preCICE is performing poorly as opposed to the legacy coupling. Hence, we extend the Pantha drying case to have more particles and CFD cells for a numerical experiment. This still keeps the underlying physics the same while allowing the study of performance for a computationally heavier case. The particle sizes are reduced, and we pack $23,999$ particles in the domain. The CFD mesh is further discretized to have $4,800$ cells.

Figure 21 shows the performance for the different coupling. The first notable observation when comparing figure 21 (a) versus (b) and (d) versus (e), is that with the scaled-up cases, the legacy coupling and preCICE serial coupling are closely matched. Furthermore, the increased load shows the disparity between staggered and simultaneous execution. The figure 21 (c) and (f), shows that the simultaneous execution of the solver gives a substantial performance advantage. As the CFD load is still quite small compared to the DEM load, it can be seen that the CFD solver spends a lot of time

36

753 idling, especially in figure 21 (c). As the number of computing resources is
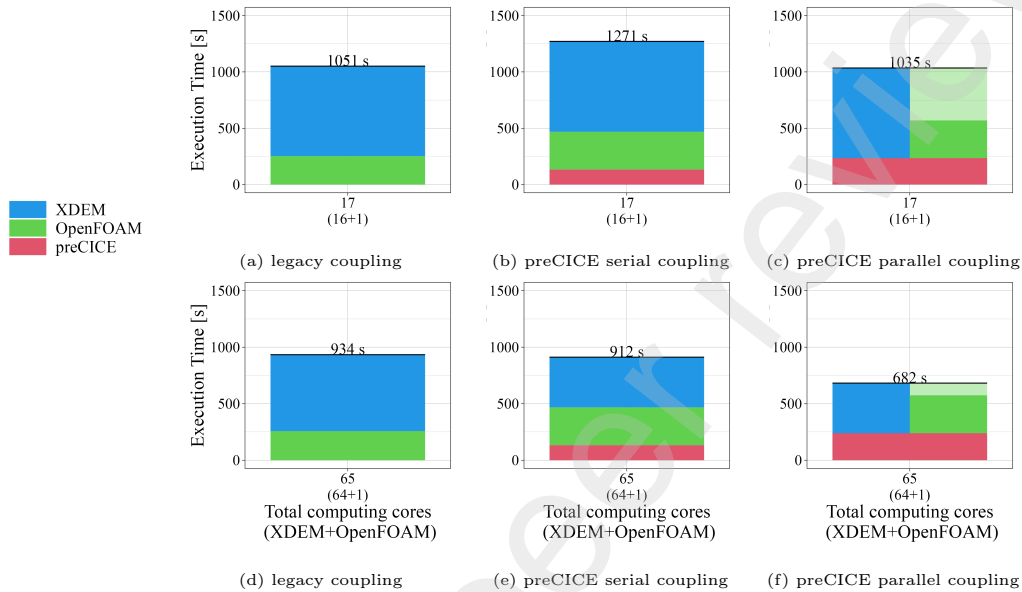**754** increased, this idling time is reduced in figure 21 (f), but still present.

Figure 21: Performance comparison of the large case for the legacy coupling vs the pre-CICE serial and parallel coupling

755 **6. Discussion**

756   The results presented in the sections 4, illustrate beyond any doubt that
757 the partitioned coupling approach presented in this work can capture the
758 multi-physics behavior. The minor differences in the numerical results be-
759 tween the legacy coupling and the proposed partitioned coupling are to be
760 expected due to the different implementations of the OpenFOAM used along
761 with the different data mapping strategies. In our study, we compared the
762 results of the partitioned coupling approach to experimental data, as well as
763 with the numerical simulation results obtained using the monolithic legacy
764 coupling. The results are in good agreement with the experimental observa-
765 tions as well as the legacy coupling. This is the case for simple single-particle
766 cases as well as packed beds.
767   The volumetric coupling employed uses a simple grid on the DEM solver
768 to exchange data to and from to the CFD solver. Hence, even when employing

37

unresolved CFD-DEM coupling, the CFD mesh size is no longer dependent on and limited by the largest particle. This opens up avenues to explore applications in need of refined CFD mesh smaller than the particles without the need to use resolved CFD-DEM coupling.

Along with the verified and validated numerical results, this type of coupling gives us the advantage of modularity and flexibility. As the solvers are not intermingled, one solver can be easily swapped out for the other. Furthermore, we would like to point out that now the software language is also no more a restriction. Highly optimized solvers are usually developed in C++, whereas experimental and research implementations are done in Mat-LAB or Python, or similar high-level language. Using the preCICE coupling library these solvers implemented in different programming languages can be coupled without any intrusion. Although it is possible to implement monolithic solvers with some functionalities presented in the coupling section 3, the amount of work needed to do so is substantial. This work demonstrates that single-physics numerical solvers can now be coupled with another single-physics software to achieve a coupled multi-physics simulation environment.

Additionally, the performance study for a packed bed is presented. With the two cases presented, we show that the performance is dependent on case to case, and the computational resources allocated. It is also shown that the partitioned coupling approach scales well, and performs just as well as the legacy coupling or even better when executing the solvers simultaneously. There are also restrictions on partitioning when using monolithic coupling. Apart from the issue of non-conforming meshes, as presented in section 5 there might be cases where the partitioning and resource allocation needs of the two involved solvers are different. When employing partitioned coupling, the parallelization capabilities of the individual solvers can be utilised to the fullest.

The monolithic coupling approach solves the set of equations in the same solver. This means that both the solvers involved have to use the same time-step. This time-step is usually dictated by the unstable solver, where reducing the time-step size leads to stability. However, due to the nature of the monolithic coupling, one solver is executed at lower time steps and penalized in computational time due to the unstable solver. When using the partitioned coupling approach, the individual solver time steps are independent of each other, however, they cannot be more than the coupling time-step. This way, the stable solver can retain its time-step, while the unstable solver can utilize a lower time-step for stability. Furthermore, more

38

807 computational resources can be allocated to the solver with a lower time-step,
808 to balance the computational load.

809 The current approach solves several issues faced in the state of the art
810 for the development of coupled simulation environment. With this work, the
811 authors intend to demonstrate the capabilities and flexibility of using the
812 partitioned coupling approach. We believe that our findings will be useful
813 for researchers and practitioners working in the field of particulate matter
814 processes, particularly those interested in modeling CFD-DEM multi-physics
815 simulations.

816 As a part of future work, this HMT coupling is to be applied to large-scale
817 applications such as blast furnaces and biomass furnaces. A thorough study
818 of the performance and the load balancing challenges using this partitioned
819 coupling approach is to be done [44]. These cases also involve the motion of
820 the particles along with the heat and mass transfer processes.

7. Conclusion

822 In this work, we present the rapid development of the simulation environ-
823 ment for HMT coupling between CFD and DEM. With the flexibility from
824 preCICE, a user can switch the CFD solver for a preferred one or they can
825 modify OpenFOAM solvers for preferred functionality. In any scenario, this
826 kind of coupling allows the user to test out HMT coupling between particles
827 and fluids. The user may use their own tested, proven, validated CFD or
828 DEM solver to replace the software used in this work to achieve CFD-DEM
829 coupling and simulate desired HMT processes. With the presented results, it
830 is seen that the flexible CFD-DEM black box coupling has similar if not the
831 same results as a specialized CFD-DEM solver. The numerical results are in
832 good agreement with the experimental observations.

833 Heat and mass transfer modules are added to the XDEM and OpenFOAM
834 adapters with relevant required data fields to be exchanged. This enables the
835 rapid development of a multi-physics environment for HMT between particles
836 (DEM) and fluids (CFD). Simple cases are employed to prove that the HMT
837 coupling is working properly. The numerical simulation results are validated
838 against the experimental results, and they are in good agreement. Thus prov-
839 ing HMT coupling using preCICE works i.e. two-way HMT coupling between
840 CFD (OpenFOAM) and DEM (XDEM). This opens up opportunities for the
841 simulation of HMT processes such as drying, gasification, combustion, and
842 pyrolysis.

39

In the HMT validation case, we use chemical species H2O, O2, N2, but our adapter also supports other species such as CH4, CO2, CO, H2, Tar commonly used in the biomass combustion process, or iron making processes. Although these species cover a wide range of applications, one might still need to use many different chemical species. We are working on automating the exchanged species based on fields defined in the preCICE configuration.

This work was limited to HMT applications involving gaseous fluid mixtures. To simulate processes such as melting, and phase change, the Open-FOAM adapter, XDEM adapter, and XDEM have to be updated to handle multiphase Euler-type CFD solvers.

The proposed partitioned coupling approach performs just as well or better than the legacy coupling for large-scale simulations. Thus this type of coupling is scalable and applicable to large-scale applications.

In future work, we validate individual processes such as gasification, and combustion similar to the drying and pyrolysis process in the current work. Complex cases such as biomass furnaces and blast furnaces are being investigated using the current implementation and are being validated.

Acknowledgment

References

[1] Bernhard Peters et al. "XDEM multi-physics and multi-scale simulation technology: Review of DEM–CFD coupling, methodology and engineering applications". In: *Particuology* 44 (2019), pp. 176–193.

[2] HP Zhu et al. "Discrete particle simulation of particulate systems: a review of major applications and findings". In: *Chemical Engineering Science* 63.23 (2008), pp. 5728–5770.

[3] Andrew Hobbs. "Simulation of an aggregate dryer using coupled CFD and DEM methods". In: *International Journal of Computational Fluid Dynamics* 23.2 (2009), pp. 199–207.

40

[4] F Sudbrock et al. "Convective drying of agitated silica gel and beech wood particle beds—experiments and transient DEM-CFD simulations". In: *Drying technology* 33.15-16 (2015), pp. 1808–1820.

[5] Patiwat Khomwachirakul et al. "Simulation of flow and drying characteristics of high-moisture particles in an impinging stream dryer via CFD-DEM". In: *Drying technology* 34.4 (2016), pp. 403–419.

[6] Viktor Scherer et al. "Coupled DEM–CFD simulation of drying wood chips in a rotary drum–Baffle design and model reduction". In: *Fuel* 184 (2016), pp. 896–904.

[7] Matthias Börner, Andreas Bück, and Evangelos Tsotsas. "DEM-CFD investigation of particle residence time distribution in top-spray fluidised bed granulation". In: *Chemical Engineering Science* 161 (2017), pp. 187–197.

[8] Daoyin Liu, Changsheng Bu, and Xiaoping Chen. "Development and test of CFD–DEM model for complex geometry: A coupling algorithm for Fluent and DEM". In: *Computers & Chemical Engineering* 58 (2013), pp. 260–268. ISSN: 0098-1354. DOI: https://doi.org/10.1016/j.compchemeng.2013.07.006.

[9] Clarissa B Fonte, JA Oliveira Jr, and Lucilla C de ALMEIDA. "DEM-CFD coupling: mathematical modelling and case studies using ROCKY-DEM® and ANSYS Fluent®". In: *Proceedings of the 11th International Conference on CFD in the Minerals and Process Industries, CSIRO, Melbourne, Australia.* 2015, pp. 7–9.

[10] Christoph Goniva et al. "Open source CFD-DEM modelling for particle-based processes". In: *11th International Conference on Computational Fluid Dynamics in the Minerals and Process Industries.* 2015.

[11] Kristin Kerst et al. "CFD-DEM simulations of a fluidized bed crystallizer". In: *Chemical Engineering Science* 165 (2017), pp. 1–13.

[12] Maryam Askarishahi, Mohammad-Sadegh Salehi, and Stefan Radl. "Full-physics simulations of spray-particle interaction in a bubbling fluidized bed". In: *AIChE Journal* 63.7 (2017), pp. 2569–2587.

[13] Benjamin Walter Uekermann. "Partitioned fluid-structure interaction on massively parallel systems". PhD thesis. Technische Universität München, 2016.

41

[14]   Shahab Golshan et al. "Review and implementation of CFD-DEM applied to chemical process systems". In: *Chemical Engineering Science* 221 (2020), p. 115646.

[15]   Xavier Besseron, Henrik Rusche, and Bernhard Peters. "Parallel Multi-Physics Simulation of Biomass Furnace and Cloud-based Workflow for SMEs". English. In: *Practice and Experience in Advanced Research Computing (PEARC '22)*. CE - Commission Européenne [BE]. Boston, MA, United States: Association for Computing Machinery, July 2022. DOI: 10.1145/3491418.3530294. URL: https://pearc.acm.org/pearc22/.

[16]   Gabriele Pozzetti et al. "A co-located partitions strategy for parallel CFD–DEM couplings". In: *Advanced Powder Technology* 29.12 (2018), pp. 3220–3232.

[17]   Gerasimos Chourdakis et al. "preCICE v2: A sustainable and user-friendly coupling library". In: *Open Research Europe* 2 (2022).

[18]   *preCICE Coupling Library official page*. URL: www.precice.org. (accessed: 2020).

[19]   Gerasimos Chourdakis, David Schneider, and Benjamin Uekermann. "OpenFOAM-preCICE: Coupling OpenFOAM with External Solvers for Multi-Physics Simulations". In: *OpenFOAM® Journal* 3 (2023), pp. 1–25.

[20]   Gerasimos Chourdakis et al. "Coupling OpenFOAM to different solvers, physics, models, and dimensions using preCICE". en. In: *14th Open-FOAM Workshop*. Duisburg, Germany, July 2019. URL: https://www.conftool.com/ofw14/index.php?page=browseSessions%5C&form_session=26%5C&presentations=show.

[21]   Lucia Cheung Yau. "Conjugate Heat Transfer with the Multiphysics Coupling Library preCICE". Master's thesis. Technical University of Munich, 2016.

[22]   Patrick Schmidt et al. "Simulation of flow in deformable fractures using a quasi-Newton based partitioned coupling approach". In: *Computational Geosciences* (2022). ISSN: 15731499. DOI: 10.1007/s10596-021-10120-8.

42

[23] Mehdi Baniasadi, Maryam Baniasadi, and Bernhard Peters. "Coupled CFD-DEM with heat and mass transfer to investigate the melting of a granular packed bed". In: *Chemical Engineering Science* 178 (2018), pp. 136–145.

[24] Jiaxin Cui, Qinfu Hou, and Yansong Shen. "CFD-DEM study of coke combustion in the raceway cavity of an ironmaking blast furnace". In: *Powder Technology* 362 (2020), pp. 539–549.

[25] Christian Bruch, Bernhard Peters, and Thomas Nussbaumer. "Modelling wood combustion under fixed bed conditions". In: *Fuel* 82.6 (2003), pp. 729–738.

[26] Amir Houshang Mahmoudi, Florian Hoffmann, and Bernhard Peters. "Application of XDEM as a novel approach to predict drying of a packed bed". In: *International Journal of Thermal Sciences* 75 (2014), pp. 65–75.

[27] Amir Houshang Mahmoudi et al. "An experimental and numerical study of wood combustion in a fixed bed using Euler–Lagrange approach (XDEM)". In: *Fuel* 150 (2015), pp. 573–582.

[28] *OpenFOAM Foundation*. URL: https://openfoam.org. (accessed: 2020).

[29] Gerasimos Chourdakis. "A general OpenFOAM adapter for the coupling library preCICE". MA thesis. Technical University of Munich, Oct. 2017. URL: https://www5.in.tum.de/pub/Chourdakis2017_Thesis.pdf.

[30] Amir Houshang Mahmoudi, Florian Hoffmann, and Bernhard Peters. "Semi-resolved modeling of heat-up, drying and pyrolysis of biomass solid particles as a new feature in XDEM". In: *Applied Thermal Engineering* 93 (2016), pp. 1091–1104.

[31] Bernhard Peters. *Thermal conversion of solid fuels*. eng. International series on developments in heat transfer Vol. 15 15. Southampton: WIT Press, 2003. ISBN: 1-85312-953-4.

[32] Navid Aminnia et al. "Three-dimensional CFD-DEM simulation of raceway transport phenomena in a blast furnace". In: *Fuel* 334 (2023), p. 126574.

[33] Bernhard Peters. "Thermal conversion of solid fuels". In: (2002).

43

[34] Benjamin Uekermann et al. "Official preCICE adapters for standard open-source solvers". In: *Proceedings of the 7th GACM colloquium on computational mechanics for young scientists from academia*. 2017.

[35] E Achenbach. "Heat and flow characteristics of packed beds". In: *Experimental thermal and fluid science* 10.1 (1995), pp. 17–27.

[36] Volker Gnielinski. "New equations for heat and mass transfer in turbulent pipe and channel flow". In: *International chemical engineering* 16.2 (1976), pp. 359–367.

[37] Jian Yang et al. "Experimental analysis of forced convective heat transfer in novel structured packed beds of particles". In: *Chemical engineering science* 71 (2012), pp. 126–137.

[38] Noriaki Wakao and Seiichirō Kagei. *Heat and mass transfer in packed beds*. Vol. 1. Taylor & Francis, 1982.

[39] Hans-Joachim Bungartz et al. "preCICE – A fully parallel library for multi-physics surface coupling". In: *Computers and Fluids* 141 (2016). Advances in Fluid-Structure Interaction, pp. 250–258. ISSN: 0045-7930. DOI: https://doi.org/10.1016/j.compfluid.2016.04.003.

[40] Bernhard Peters et al. "Measurements and particle resolved modelling of heat-up and drying of a packed bed". In: *Biomass and Bioenergy* 23.4 (2002), pp. 291–306.

[41] *Foam Extend v3.2*. URL: https://openfoamwiki.net/index.php/Installation/Linux/foam-extend-3.2. (accessed: 2020).

[42] Josef Petek. *Experimentelle Untersuchung der Pyrolyse in inerter und reaktiver Atmosphäre unter den Bedingungen der Wurfbeschickung*. na, 1998.

[43] Bernhard Peters and Christian Bruch. "Drying and pyrolysis of wood particles: experiments and simulation". In: *Journal of analytical and applied pyrolysis* 70.2 (2003), pp. 233–250.

[44] Xavier Besseron, Prasad Adhav, and Bernhard Peters. "Parallel Multi-Physics Coupled Simulation of a Midrex Blast Furnace". In: *Proceedings of the HPC Asia 2024 Workshops*. New York, NY, United States: Association for Computing Machinery, 2024. DOI: XX.XXX/XXXXXXX.XXXXXXX.

44

₁₀₀₉ **Nomenclature**

Scalars

c_p	Specific Heat $(J/(Kg.K))$
d	Particle diameter (m)
I_i	Moment of inertia $(kg.m^2)$
m	Mass (kg)
m'	Mass source $(kg/m^3.s)$
p	Pressure (Pa)
q'	Heat source (W/m^2)
q''	Heat flux (W/m^2)
r, R	Radius (m)
t	Time (s)
T	Temperature (K)
₁₀₁₀ T_{final}	Length of simulation (s)

First order tensor (vectors)

$\vec{g}$	Acceleration due to gravity (m/s)
$\vec{F^c}$	Contact Forces (N)
$\vec{F^g}$	Gravitational Force (N)
$\vec{F^{ext}}$	External Forces (N)
$\vec{F_B}$	Buoyancy Force (N)
$\vec{F_D}$	Drag Force (N)
$\vec{M_{i,j}}$	torque generated by inter-particle forces $(N.m)$
$\vec{S}$	Momentum source due particles
$\vec{v}_f$	Fluid velocity field
$\vec{X_i}$	Positional vector (m)
$\vec{\omega}$	Rotational velocity (rad/s)

Greek symbols

α	Heat transfer coefficient $(W/(m.K))$
β	Momentum exchange $(kg/(m^3.s))$
∂	Differential operator (-)
ϵ	Volume Fraction/Porosity (-)
μ	Kinematic viscosity $(Pa.s)$
∇	Nabla operator (-)
ρ	Density (kg/m^3)

Subscripts

c	Cell
$cond$	Conduction
eff	Effective values
f	Fluid
i, j	Particle
n	Normal direction
p, P	Particle
rad	Radiation
t	Tangential direction

45